THE ASTROPHYSICAL JOURNAL SUPPLEMENT SERIES, 113:69–88, 1997 November


# STEPS TOWARD DETERMINATION OF THE SIZE AND STRUCTURE OF THE BROAD-LINE REGION IN ACTIVE GALACTIC NUCLEI. XI. INTENSIVE MONITORING OF THE ULTRAVIOLET SPECTRUM OF NGC 7469

I. WANDERS,[1,2] B. M. PETERSON,[1] D. ALLOIN,[3] T. R. AYRES,[4] J. CLAVEL,[5] D. M. CRENSHAW,[6] K. HORNE,[2] G. A. KRISS,[7] J. H. KROLIK,[7] M. A. MALKAN,[8] H. NETZER,[9] P. T. O'BRIEN,[10] G. A. REICHERT,[11] P. M. RODRÍGUEZ-PASCUAL,[12] W. WAMSTEKER,[12] T. ALEXANDER,[9,13] K. S. J. ANDERSON,[14] E. BENITEZ,[15] N. G. BOCHKAREV,[16] A. N. BURENKOV,[17] F.-Z. CHENG,[18] S. J. COLLIER,[2] A. COMASTRI,[19] M. DIETRICH,[20] D. DULTZIN-HACYAN,[15] B. R. ESPEY,[7] A. V. FILIPPENKO,[21] C. M. GASKELL,[22] I. M. GEORGE,[23,24] M. R. GOAD,[25] L. C. HO,[26] S. KASPI,[9] W. KOLLATSCHNY,[27] K. T. KORISTA,[28] A. LAOR,[29] G. M. MACALPINE,[30] M. MIGNOLI,[19] S. L. MORRIS,[31] K. NANDRA,[23,24] S. PENTON,[4] R. W. POGGE,[1] R. L. PTAK,[32] J. M. RODRÍGUEZ-ESPINOZA,[33] M. SANTOS-LLEÓ,[34] A. I. SHAPOVALOVA,[17] J. M. SHULL,[35] S. A. SNEDDEN,[22] L. S. SPARKE,[36] G. M. STIRPE,[19] W.-H. SUN,[37] T. J. TURNER,[23,24] M.-H. ULRICH,[38] T.-G. WANG,[18] C. WEI,[26] W. F. WELSH,[39] S.-J. XUE,[18] AND Z.-L. ZOU[40]

*Received 1997 March 24; accepted 1997 May 5*

## ABSTRACT

From 1996 June 10 to July 29, the *International Ultraviolet Explorer* monitored the Seyfert 1 galaxy NGC 7469 continuously in an attempt to measure time delays between the continuum and emission-line fluxes. From the time delays, one can estimate the size of the region dominating the production of the UV emission lines in this source. We find the strong UV emission lines to respond to continuum variations with time delays of about $2\overset{d}{.}3$–$3\overset{d}{.}1$ for Ly$\alpha$, $2\overset{d}{.}7$ for C IV $\lambda$1549, $1\overset{d}{.}9$–$2\overset{d}{.}4$ for N V $\lambda$1240, $1\overset{d}{.}7$–$1\overset{d}{.}8$ for Si IV $\lambda$1400, and $0\overset{d}{.}7$–$1\overset{d}{.}0$ for He II $\lambda$1640. The most remarkable result, however, is the detection of apparent time delays between the different UV continuum bands. With respect to the UV continuum flux at 1315 Å, the flux at 1485 Å, 1740 Å, and 1825 Å lags with time delays of $0\overset{d}{.}21$, $0\overset{d}{.}35$, and $0\overset{d}{.}28$, respectively. Determination of the significance of this detection is somewhat problematic since it depends on accurate estimation of the uncertainties in the lag measurements, which are difficult to assess. We attempt to estimate the uncertainties in the time delays through Monte Carlo simulations, and these yield estimates of $\sim 0\overset{d}{.}07$ for the 1 $\sigma$ uncertainties in the interband continuum time delays. Possible explanations for the delays include the existence of a continuum-flux reprocessing region close to the central source and/or a contamination of the continuum flux with a very broad time-delayed emission feature such as the Balmer continuum or merged Fe II multiplets.

*Subject headings:* galaxies: active — galaxies: individual (NGC 7469) — galaxies: Seyfert — ultraviolet: galaxies

## 1. INTRODUCTION

Numerous studies of flux variations in the broad emission lines of active galactic nuclei (AGNs) have established that they respond to changes in the continuum flux. This provides strong evidence for photoionization of the broad-line region (BLR) by the central continuum source. The time difference between a continuum flux variation and a broad emission-line response can be attributed to light-travel time effects through the BLR, which can be used to derive the geometric and kinematic structure of the BLR through a technique called reverberation mapping (Blandford & McKee 1982; see Peterson 1993 for a review).

Reverberation mapping requires high temporal sampling of a variable AGN at high signal-to-noise ratios, over as long a time span as possible. The *International Ultraviolet Explorer* (*IUE*) has been well suited for this task, partly because it can monitor AGNs without interruptions due to weather, but primarily because the ultraviolet (UV) continuum flux varies with larger amplitude than the optical continuum flux and because several important emission lines, including Ly$\alpha$ $\lambda$1216, C IV $\lambda$1549, and He II $\lambda$1640, are emitted in the UV.

The International AGN Watch consortium (Alloin et al. 1994) has conducted several large monitoring campaigns to obtain data suitable for reverberation-mapping analysis. In 1989, continuum and emission-line variability in the Seyfert 1 galaxy NGC 5548 was monitored for 8 months with *IUE* (Clavel et al. 1991) and ground-based optical telescopes (Peterson et al. 1991; Dietrich et al. 1993; Maoz et al. 1993; Romanishin et al. 1995), which produced light curves that are sufficiently well resolved to yield time delays for many strong emission lines. These data provide strong evidence for a radially stratified ionization structure for the BLR because the low-ionization lines respond more slowly to continuum variations than do the high-ionization lines. Indeed, the response times for the highest ionization lines measured, He II $\lambda$1640 and N V $\lambda$1240, remained unresolved with the 4 day sampling interval obtained with *IUE*. An important result of this campaign was that the various measured continuum bands, from $\sim$1350 to $\sim$5200 Å, vary in phase, contrary to expectations if the continuum source has a radial temperature gradient (as expected for a thin accretion disk) or if the variations are due to disk disturbances that propagate through the disk at the sound speed

(Courvoisier & Clavel 1991; Collin-Souffrin 1991; Krolik et al. 1991). A subsequent combined *IUE*/*HST* campaign in 1993 with daily sampling showed that the very high ionization lines respond to continuum variations with time delays of about 1–3 days and placed a more stringent limit on any UV/optical continuum phase delay (Korista et al. 1995). Monitoring campaigns on other sources, such as NGC 3783 (Reichert et al. 1994; Stirpe et al. 1994) and Fairall 9 (Rodríguez-Pascual et al. 1997; Santos-Lleó et al. 1997), have led to similar results.

It is generally supposed in reverberation mapping that the light curve of an emission line $L(t)$ is related to the continuum light curve $C(t)$ through

$$\delta L(t) = \int \delta C(t - \tau)\Psi(\tau)d\tau \ , \qquad (1)$$

where $\Psi(\tau)$ is the geometry-dependent "transfer function" and $\tau$ is a time delay (Blandford & McKee 1982). One of the goals of AGN emission-line variability studies is to invert this equation, solve for $\Psi(\tau)$, and thus infer, under certain physical assumptions, the BLR geometry. Attempts to recover the emission-line transfer functions from the existing data (Horne, Welsh, & Peterson 1991; Krolik et al. 1991; Wanders et al. 1995; Krolik & Done 1995) have been only partially successful, primarily because of ambiguities that arise from having a limited number of data points for the inversion.

It must be noted that the emission-line variability is a result of the response of the BLR to the incident *ionizing* continuum radiation. This ionizing radiation is unobservable owing to the large optical depth of the interstellar medium at wavelengths shorter than 912 Å. However, the close correlation between the observed UV continuum variability and the responding broad emission-line variability suggests that the observed UV continuum is a good indicator of the unobserved ionizing continuum. Throughout this paper, we use the observed UV continuum as if it were the ionizing continuum, as is common practice in reverberation studies of AGNs.

The close coupling of the variations in the various continuum bands and the necessity of obtaining larger data sets for the recovery of the transfer function have led to progressively larger monitoring programs. In 1994 December, a very intensive 10 day multiwavelength monitoring program on NGC 4151 was carried out (Crenshaw et al. 1996; Kaspi et al. 1996; Warwick et al. 1996; Edelson et al. 1996). This experiment led to small upper limits on any wavelength-dependent phase difference in the continuum variations (less than $\sim 0^{d}.15$ between 1275 Å and other UV bands, less than $\sim 0^{d}.3$ between 1275 Å and 1.5 keV, and less than $\sim 1$ day between 1275 Å and 5125 Å), but the relatively short duration of the experiment (and consequently low amplitude of line variability) did not yield useful information about the emission-line response.

[1] Department of Astronomy, The Ohio State University, 174 West 18th Avenue, Columbus, OH 43210.
[2] School of Physics and Astronomy, University of St. Andrews, North Haugh, St. Andrews KY16 9SS, Scotland, United Kingdom.
[3] Centre d'Etudes de Saclay, Service d'Astrophysique, Orme des Merisiers, 91191 Gif-sur-Yvette Cedex, France.
[4] Center for Astrophysics and Space Astronomy, University of Colorado, Campus Box 389, Boulder, CO 80309.
[5] ISO Project, European Space Agency, Apartado 50727, 28080 Madrid, Spain.
[6] Computer Sciences Corporation, Laboratory for Astronomy and Solar Physics, NASA Goddard Space Flight Center, Code 681, Greenbelt, MD 20771.
[7] Department of Physics and Astronomy, The Johns Hopkins University, Baltimore, MD 21218.
[8] Department of Astronomy, University of California, Math-Science Building, Los Angeles, CA 90024.
[9] School of Physics and Astronomy and the Wise Observatory, The Raymond and Beverly Sackler Faculty of Exact Sciences, Tel-Aviv University, Tel-Aviv 69978, Israel.
[10] Department of Physics and Astronomy, University of Leicester, University Road, Leicester LE1 7RH, United Kingdom.
[11] NASA Goddard Space Flight Center, Code 631, Greenbelt, MD 20771.
[12] ESA IUE Observatory, P.O. Box 50727, 28080 Madrid, Spain.
[13] Max-Planck-Institut für extraterrestrische Physik, Postfach 1603, 85740 Garching, Germany.
[14] Department of Astronomy, New Mexico State University, Box 30001, Department 4500, Las Cruces, NM 88003.
[15] Universidad Nacional Autonoma de Mexico, Instituto de Astronomia, Apartado Postal 70-264, 04510 Mexico D.F., Mexico.
[16] Sternberg Astronomical Institute, University of Moscow, Universitetskij Prosp. 13, Moscow 119899, Russia.
[17] Special Astrophysical Observatory, Russian Academy of Sciences, Nizhnij Arkhyz, Karachaj-Cherkess Republic, 357147, Russia.
[18] Center for Astrophysics, University of Science and Technology, Hefei, Anhui, People's Republic of China.
[19] Osservatorio Astronomico di Bologna, Via Zamboni 33, I-40126, Bologna, Italy.
[20] Landessternwarte, Königstuhl, D-69117 Heidelberg, Germany.
[21] Department of Astronomy, University of California, Berkeley, Berkeley, CA 94720.
[22] Department of Physics and Astronomy, University of Nebraska, Lincoln, NE 68588.
[23] Laboratory for High Energy Astrophysics, NASA Goddard Space Flight Center, Greenbelt, MD 20771.
[24] Universities Space Research Association.
[25] Space Telescope Science Institute, 3700 San Martin Drive, Baltimore, MD 21218.
[26] Harvard-Smithsonian Center for Astrophysics, 60 Garden Street, Cambridge, MA 02138.
[27] Universitäts-Sternwarte Göttingen, Geismarlandstrasse 11, D-37083 Göttingen, Germany.
[28] Department of Physics and Astronomy, University of Kentucky, Lexington, KY 40506.
[29] Physics Department, Technion-Israel Institute of Technology, Haifa 32000, Israel.
[30] Department of Astronomy, University of Michigan, Dennison Building, Ann Arbor, MI 48109.
[31] Dominion Astrophysical Observatory, 5071 West Saanich Road, Victoria, B.C. V8X 4M6, Canada.
[32] Department of Physics and Astronomy, Bowling Green State University, Bowling Green, OH 43403.
[33] Instituto de Astrofisica de Canarias, E-38200 La Laguna, Tenerife, Spain.
[34] LAEFF, Apdo. 50727, E-28080 Madrid, Spain.
[35] Joint Institute for Laboratory Astrophysics, University of Colorado, and National Institute of Standards and Technology, Campus Box 440, Boulder, CO 80309.
[36] Department of Astronomy, University of Wisconsin, 475 North Charter Street, Madison, WI 53706.
[37] Institute of Astronomy, National Central University, Chung-Li, Taiwan 32054, Republic of China.
[38] European Southern Observatory, Karl Schwarzschild Strasse 2, 85748 Garching, Germany.
[39] McDonald Observatory and Department of Astronomy, University of Texas, RLM 15.308, Austin, TX 78712.
[40] Beijing Astronomical Observatory, Chinese Academy of Sciences, Beijing 100080, People's Republic of China.

TABLE 1

LOG OF OBSERVATIONS

| Image (SWP Number) (1) | Observation Date (UT 1996) (2) | Start of Observation Time (UT hh:mm:ss) (3) | Exposure Time (s) (4) | JD (−2,450,000) (5) | Exposure Time (days) (6) | Notes[a] (7) |
|---|---|---|---|---|---|---|
| 57382 | Jun 10 | 13:57:37 | 2700 | 245.10 | 0.031 | 1 |
| 57383 | Jun 10 | 23:53:46 | 9000 | 245.55 | 0.104 | 2 |
| 57384 | Jun 11 | 04:07:28 | 9000 | 245.72 | 0.104 | |
| 57385 | Jun 11 | 08:27:28 | 9000 | 245.90 | 0.104 | |
| 57386 | Jun 11 | 13:08:29 | 1740 | 246.06 | 0.020 | 3 |
| 57389 | Jun 12 | 01:19:23 | 9000 | 246.61 | 0.104 | |
| 57390 | Jun 12 | 05:48:59 | 9000 | 246.79 | 0.104 | |
| 57391 | Jun 12 | 09:57:31 | 9000 | 246.97 | 0.104 | |
| 57395 | Jun 13 | 00:21:39 | 9000 | 247.57 | 0.104 | |
| 57396 | Jun 13 | 04:35:14 | 9000 | 247.74 | 0.104 | |
| 57397 | Jun 13 | 09:09:27 | 9000 | 247.93 | 0.104 | |
| 57398 | Jun 13 | 20:44:58 | 9000 | 248.42 | 0.104 | |
| 57399 | Jun 14 | 01:14:50 | 9000 | 248.60 | 0.104 | |
| 57400 | Jun 14 | 05:31:40 | 9000 | 248.78 | 0.104 | |
| 57401 | Jun 14 | 09:48:34 | 9000 | 248.96 | 0.104 | |
| 57402 | Jun 14 | 14:54:42 | 4320 | 249.15 | 0.050 | 3 |
| 57403 | Jun 14 | 20:09:35 | 9000 | 249.39 | 0.104 | |
| 57404 | Jun 15 | 00:23:19 | 9000 | 249.57 | 0.104 | |
| 57405 | Jun 15 | 04:27:53 | 9000 | 249.74 | 0.104 | |
| 57406 | Jun 15 | 08:47:31 | 9000 | 249.92 | 0.104 | |
| 57407 | Jun 15 | 13:08:08 | 3420 | 250.07 | 0.040 | 3 |
| 57408 | Jun 15 | 20:44:59 | 9000 | 250.42 | 0.104 | |
| 57409 | Jun 16 | 00:50:51 | 9000 | 250.59 | 0.104 | |
| 57410 | Jun 16 | 04:57:28 | 9000 | 250.76 | 0.104 | |
| 57411 | Jun 16 | 08:56:54 | 9000 | 250.92 | 0.104 | |
| 57412 | Jun 16 | 22:16:32 | 9000 | 251.48 | 0.104 | |
| 57413 | Jun 17 | 02:27:48 | 9000 | 251.65 | 0.104 | |
| 57414 | Jun 17 | 06:17:58 | 9000 | 251.81 | 0.104 | |
| 57415 | Jun 17 | 10:31:26 | 9000 | 251.99 | 0.104 | |
| 57416 | Jun 17 | 21:28:08 | 9000 | 252.45 | 0.104 | |
| 57419 | Jun 18 | 05:24:24 | 9000 | 252.78 | 0.104 | |
| 57420 | Jun 18 | 09:35:42 | 9000 | 252.95 | 0.104 | |
| 57421 | Jun 18 | 20:20:54 | 9000 | 253.40 | 0.104 | |
| 57422 | Jun 19 | 00:28:12 | 9000 | 253.57 | 0.104 | |
| 57423 | Jun 19 | 04:24:41 | 9000 | 253.74 | 0.104 | |
| 57424 | Jun 19 | 08:31:21 | 9000 | 253.91 | 0.104 | |
| 57425 | Jun 19 | 12:37:27 | 1893 | 254.04 | 0.022 | 3 |
| 57426 | Jun 19 | 20:09:40 | 9000 | 254.39 | 0.104 | |
| 57427 | Jun 20 | 00:09:35 | 9000 | 254.56 | 0.104 | |
| 57428 | Jun 20 | 04:07:37 | 9000 | 254.72 | 0.104 | |
| 57429 | Jun 20 | 08:16:02 | 9000 | 254.90 | 0.104 | |
| 57430 | Jun 20 | 20:39:45 | 9000 | 255.41 | 0.104 | |
| 57431 | Jun 21 | 00:59:32 | 9000 | 255.59 | 0.104 | |
| 57432 | Jun 21 | 05:00:41 | 9000 | 255.76 | 0.104 | |
| 57433 | Jun 21 | 09:01:38 | 9000 | 255.93 | 0.104 | |
| 57434 | Jun 21 | 20:40:19 | 9000 | 256.41 | 0.104 | |
| 57435 | Jun 22 | 08:51:31 | 9000 | 256.92 | 0.104 | |
| 57436 | Jun 22 | 20:42:24 | 9000 | 257.41 | 0.104 | 2 |
| 57439 | Jun 23 | 06:19:53 | 9000 | 257.82 | 0.104 | |
| 57440 | Jun 23 | 10:09:22 | 9000 | 257.98 | 0.104 | |
| 57441 | Jun 23 | 20:35:48 | 9000 | 258.41 | 0.104 | |
| 57442 | Jun 24 | 00:39:28 | 9000 | 258.58 | 0.104 | |
| 57443 | Jun 24 | 04:50:54 | 9000 | 258.75 | 0.104 | |
| 57444 | Jun 24 | 09:08:43 | 9000 | 258.93 | 0.104 | |
| 57445 | Jun 24 | 20:13:57 | 9000 | 259.40 | 0.104 | |
| 57446 | Jun 25 | 00:42:50 | 9000 | 259.58 | 0.104 | |
| 57447 | Jun 25 | 04:53:31 | 9000 | 259.76 | 0.104 | |
| 57448 | Jun 25 | 09:40:52 | 9000 | 259.96 | 0.104 | |
| 57449 | Jun 25 | 20:28:54 | 9000 | 260.41 | 0.104 | |
| 57450 | Jun 26 | 00:54:00 | 9000 | 260.59 | 0.104 | |
| 57451 | Jun 26 | 05:27:23 | 9000 | 260.78 | 0.104 | |
| 57452 | Jun 26 | 09:40:47 | 9000 | 260.96 | 0.104 | |
| 57453 | Jun 26 | 20:03:54 | 9000 | 261.39 | 0.104 | |
| 57454 | Jun 26 | 23:16:13 | 9000 | 261.52 | 0.104 | 2 |
| 57455 | Jun 27 | 08:33:39 | 9000 | 261.91 | 0.104 | |
| 57456 | Jun 27 | 11:29:00 | 7093 | 262.02 | 0.082 | |
| 57457 | Jun 28 | 02:37:54 | 9000 | 262.66 | 0.104 | |
| 57458 | Jun 28 | 07:04:56 | 9000 | 262.85 | 0.104 | |
| 57459 | Jun 28 | 11:48:49 | 3600 | 263.01 | 0.042 | 3 |
| 57460 | Jun 28 | 19:47:32 | 9000 | 263.38 | 0.104 | |

TABLE 1—*Continued*

| Image (SWP Number) (1) | Observation Date (UT 1996) (2) | Start of Observation Time (UT hh:mm:ss) (3) | Exposure Time (s) (4) | JD (−2,450,000) (5) | Exposure Time (days) (6) | Notes[a] (7) |
|---|---|---|---|---|---|---|
| 57461 | Jun 28 | 23:57:04 | 9000 | 263.55 | 0.104 | |
| 57462 | Jun 29 | 04:02:14 | 9000 | 263.72 | 0.104 | |
| 57463 | Jun 29 | 08:09:19 | 9000 | 263.89 | 0.104 | |
| 57464 | Jun 29 | 19:43:56 | 9000 | 264.37 | 0.104 | |
| 57465 | Jun 29 | 23:50:18 | 9000 | 264.55 | 0.104 | |
| 57466 | Jun 30 | 03:30:20 | 4320 | 264.70 | 0.050 | |
| 57467 | Jun 30 | 08:39:05 | 9000 | 264.91 | 0.104 | |
| 57468 | Jun 30 | 11:35:16 | 9000 | 265.02 | 0.104 | |
| 57469 | Jun 30 | 19:36:01 | 9000 | 265.37 | 0.104 | |
| 57470 | Jun 30 | 23:22:10 | 9000 | 265.53 | 0.104 | |
| 57471 | Jul 1 | 03:04:19 | 9000 | 265.68 | 0.104 | |
| 57472 | Jul 1 | 06:50:50 | 9000 | 265.84 | 0.104 | |
| 57474 | Jul 1 | 19:55:01 | 9000 | 266.38 | 0.104 | |
| 57475 | Jul 1 | 23:44:11 | 9000 | 266.54 | 0.104 | |
| 57476 | Jul 2 | 03:25:04 | 9000 | 266.69 | 0.104 | |
| 57477 | Jul 2 | 07:06:12 | 9000 | 266.85 | 0.104 | |
| 57478 | Jul 2 | 10:55:19 | 9000 | 267.01 | 0.104 | |
| 57479 | Jul 2 | 19:34:55 | 9000 | 267.37 | 0.104 | |
| 57480 | Jul 2 | 22:31:30 | 9000 | 267.49 | 0.104 | |
| 57481 | Jul 3 | 03:47:11 | 9000 | 267.71 | 0.104 | |
| 57482 | Jul 3 | 06:52:14 | 9000 | 267.84 | 0.104 | |
| 57483 | Jul 3 | 09:50:24 | 9000 | 267.96 | 0.104 | |
| 57484 | Jul 3 | 19:41:22 | 9000 | 268.37 | 0.104 | |
| 57485 | Jul 3 | 22:45:26 | 9000 | 268.50 | 0.104 | |
| 57486 | Jul 4 | 03:59:04 | 9000 | 268.72 | 0.104 | |
| 57487 | Jul 4 | 06:56:47 | 9000 | 268.84 | 0.104 | |
| 57488 | Jul 4 | 09:55:08 | 9000 | 268.97 | 0.104 | |
| 57489 | Jul 4 | 19:40:25 | 9000 | 269.37 | 0.104 | |
| 57490 | Jul 4 | 22:50:04 | 9899 | 269.51 | 0.115 | |
| 57491 | Jul 5 | 04:25:55 | 9899 | 269.74 | 0.115 | |
| 57492 | Jul 5 | 07:50:43 | 9899 | 269.88 | 0.115 | |
| 57493 | Jul 5 | 11:18:57 | 5220 | 270.00 | 0.060 | 4 |
| 57494 | Jul 5 | 19:45:12 | 9000 | 270.38 | 0.104 | |
| 57495 | Jul 5 | 22:39:49 | 9899 | 270.50 | 0.115 | |
| 57496 | Jul 6 | 04:23:08 | 9000 | 270.73 | 0.104 | |
| 57497 | Jul 6 | 07:21:42 | 9000 | 270.86 | 0.104 | |
| 57498 | Jul 6 | 10:18:24 | 9600 | 270.98 | 0.111 | |
| 57499 | Jul 6 | 19:19:13 | 9000 | 271.36 | 0.104 | |
| 57500 | Jul 6 | 22:21:01 | 9600 | 271.49 | 0.111 | |
| 57501 | Jul 7 | 04:37:05 | 9000 | 271.74 | 0.104 | |
| 57502 | Jul 7 | 07:35:28 | 9000 | 271.87 | 0.104 | |
| 57504 | Jul 7 | 19:15:54 | 9000 | 272.35 | 0.104 | |
| 57505 | Jul 7 | 22:22:19 | 9000 | 272.48 | 0.104 | |
| 57506 | Jul 8 | 04:05:45 | 9000 | 272.72 | 0.104 | |
| 57507 | Jul 8 | 07:06:34 | 9000 | 272.85 | 0.104 | |
| 57508 | Jul 8 | 10:02:56 | 9000 | 272.97 | 0.104 | |
| 57509 | Jul 8 | 19:19:25 | 9000 | 273.36 | 0.104 | |
| 57510 | Jul 8 | 22:25:03 | 9000 | 273.49 | 0.104 | |
| 57511 | Jul 9 | 04:13:30 | 9000 | 273.73 | 0.104 | |
| 57512 | Jul 9 | 07:37:24 | 9000 | 273.87 | 0.104 | |
| 57513 | Jul 9 | 11:20:37 | 9000 | 274.02 | 0.104 | |
| 57514 | Jul 9 | 19:11:11 | 10200 | 274.36 | 0.118 | |
| 57515 | Jul 9 | 22:29:48 | 9000 | 274.49 | 0.104 | |
| 57516 | Jul 10 | 04:58:36 | 9000 | 274.76 | 0.104 | |
| 57517 | Jul 10 | 08:04:27 | 9000 | 274.89 | 0.104 | |
| 57518 | Jul 10 | 11:02:52 | 9000 | 275.01 | 0.104 | |
| 57519 | Jul 10 | 19:08:42 | 9000 | 275.35 | 0.104 | |
| 57520 | Jul 10 | 22:18:05 | 9000 | 275.48 | 0.104 | |
| 57521 | Jul 11 | 04:37:22 | 9000 | 275.74 | 0.104 | |
| 57522 | Jul 11 | 07:46:46 | 9000 | 275.88 | 0.104 | |
| 57523 | Jul 11 | 10:43:15 | 9000 | 276.00 | 0.104 | 5 |
| 57524 | Jul 11 | 19:00:45 | 9000 | 276.34 | 0.104 | |
| 57525 | Jul 11 | 22:19:20 | 9000 | 276.48 | 0.104 | |
| 57526 | Jul 12 | 04:43:15 | 9000 | 276.75 | 0.104 | |
| 57527 | Jul 12 | 07:59:13 | 9000 | 276.88 | 0.104 | 6 |
| 57528 | Jul 12 | 11:05:48 | 8100 | 277.01 | 0.094 | |
| 57529 | Jul 12 | 19:03:54 | 9000 | 277.35 | 0.104 | |
| 57530 | Jul 12 | 22:29:40 | 9000 | 277.49 | 0.104 | |
| 57531 | Jul 13 | 05:27:25 | 9000 | 277.78 | 0.104 | |
| 57532 | Jul 13 | 08:27:42 | 9000 | 277.90 | 0.104 | |
| 57533 | Jul 13 | 11:27:37 | 8400 | 278.03 | 0.097 | |

TABLE 1—*Continued*

| Image (SWP Number) (1) | Observation Date (UT 1996) (2) | Start of Observation Time (UT hh:mm:ss) (3) | Exposure Time (s) (4) | JD (−2,450,000) (5) | Exposure Time (days) (6) | Notes[a] (7) |
|---|---|---|---|---|---|---|
| 57534 | Jul 13 | 18:56:44 | 9000 | 278.34 | 0.104 | |
| 57535 | Jul 13 | 21:59:29 | 9899 | 278.47 | 0.115 | |
| 57536 | Jul 14 | 04:55:41 | 9000 | 278.76 | 0.104 | |
| 57538 | Jul 14 | 18:55:08 | 7364 | 279.33 | 0.085 | |
| 57539 | Jul 14 | 21:52:55 | 9000 | 279.46 | 0.104 | |
| 57540 | Jul 15 | 04:47:28 | 9000 | 279.75 | 0.104 | |
| 57541 | Jul 15 | 08:03:41 | 9000 | 279.89 | 0.104 | |
| 57542 | Jul 15 | 11:09:09 | 9000 | 280.02 | 0.104 | |
| 57543 | Jul 15 | 18:57:08 | 9000 | 280.34 | 0.104 | |
| 57544 | Jul 15 | 21:52:19 | 9899 | 280.47 | 0.115 | |
| 57545 | Jul 16 | 04:27:09 | 9000 | 280.74 | 0.104 | |
| 57546 | Jul 16 | 07:50:58 | 9000 | 280.88 | 0.104 | |
| 57547 | Jul 16 | 10:58:31 | 9000 | 281.01 | 0.104 | |
| 57548 | Jul 16 | 18:57:11 | 9000 | 281.34 | 0.104 | |
| 57549 | Jul 16 | 21:52:12 | 9899 | 281.47 | 0.115 | |
| 57550 | Jul 17 | 04:26:56 | 10800 | 281.75 | 0.125 | |
| 57552 | Jul 17 | 19:11:36 | 9000 | 282.35 | 0.104 | |
| 57553 | Jul 17 | 22:31:54 | 8400 | 282.49 | 0.097 | |
| 57554 | Jul 18 | 05:07:08 | 9000 | 282.77 | 0.104 | |
| 57555 | Jul 18 | 08:06:12 | 9000 | 282.89 | 0.104 | 7 |
| 57556 | Jul 18 | 11:12:46 | 8400 | 283.02 | 0.097 | |
| 57557 | Jul 18 | 18:51:08 | 9000 | 283.34 | 0.104 | |
| 57558 | Jul 18 | 21:52:54 | 9900 | 283.47 | 0.115 | |
| 57559 | Jul 19 | 04:31:04 | 9000 | 283.74 | 0.104 | |
| 57560 | Jul 19 | 07:45:56 | 9000 | 283.88 | 0.104 | |
| 57561 | Jul 19 | 10:44:10 | 9000 | 284.00 | 0.104 | |
| 57564 | Jul 19 | 19:08:01 | 9000 | 284.35 | 0.104 | 5 |
| 57565 | Jul 19 | 22:03:18 | 9000 | 284.47 | 0.104 | |
| 57566 | Jul 20 | 04:36:17 | 9000 | 284.74 | 0.104 | |
| 57567 | Jul 20 | 08:01:18 | 9000 | 284.89 | 0.104 | |
| 57568 | Jul 20 | 11:05:19 | 9000 | 285.01 | 0.104 | |
| 57569 | Jul 20 | 22:46:35 | 6600 | 285.49 | 0.076 | |
| 57570 | Jul 21 | 04:52:21 | 9000 | 285.76 | 0.104 | |
| 57571 | Jul 21 | 07:56:43 | 9000 | 285.88 | 0.104 | |
| 57572 | Jul 21 | 10:59:18 | 9000 | 286.01 | 0.104 | |
| 57574 | Jul 21 | 18:55:36 | 9000 | 286.34 | 0.104 | |
| 57575 | Jul 21 | 21:51:41 | 9899 | 286.47 | 0.115 | |
| 57576 | Jul 22 | 04:31:50 | 9000 | 286.74 | 0.104 | |
| 57577 | Jul 22 | 07:26:26 | 9000 | 286.86 | 0.104 | |
| 57578 | Jul 22 | 10:24:42 | 9000 | 286.99 | 0.104 | |
| 57579 | Jul 22 | 18:46:57 | 9000 | 287.33 | 0.104 | |
| 57580 | Jul 22 | 21:41:44 | 9899 | 287.46 | 0.115 | |
| 57581 | Jul 23 | 04:31:22 | 9000 | 287.74 | 0.104 | |
| 57582 | Jul 23 | 07:47:41 | 9000 | 287.88 | 0.104 | |
| 57583 | Jul 23 | 10:43:02 | 9000 | 288.00 | 0.104 | |
| 57584 | Jul 23 | 13:55:01 | 1508 | 288.09 | 0.017 | 3 |
| 57585 | Jul 23 | 18:55:05 | 9000 | 288.34 | 0.104 | |
| 57586 | Jul 23 | 21:51:10 | 9000 | 288.46 | 0.104 | |
| 57587 | Jul 24 | 04:24:03 | 9000 | 288.74 | 0.104 | |
| 57588 | Jul 24 | 07:32:46 | 9000 | 288.87 | 0.104 | |
| 57589 | Jul 24 | 10:33:40 | 9000 | 288.99 | 0.104 | |
| 57590 | Jul 24 | 18:53:23 | 9000 | 289.34 | 0.104 | |
| 57591 | Jul 24 | 21:49:18 | 9000 | 289.46 | 0.104 | |
| 57592 | Jul 25 | 04:20:28 | 9000 | 289.73 | 0.104 | |
| 57593 | Jul 25 | 07:39:34 | 9000 | 289.87 | 0.104 | |
| 57594 | Jul 25 | 10:43:50 | 9000 | 290.00 | 0.104 | |
| 57595 | Jul 25 | 18:47:15 | 9000 | 290.33 | 0.104 | |
| 57596 | Jul 25 | 21:43:17 | 10200 | 290.46 | 0.118 | |
| 57597 | Jul 26 | 04:12:57 | 9000 | 290.73 | 0.104 | |
| 57598 | Jul 26 | 07:40:58 | 9000 | 290.87 | 0.104 | |
| 57599 | Jul 26 | 10:45:00 | 9000 | 291.00 | 0.104 | |
| 57600 | Jul 26 | 13:42:22 | 898 | 291.08 | 0.010 | 3 |
| 57601 | Jul 26 | 18:51:05 | 9000 | 291.34 | 0.104 | |
| 57602 | Jul 26 | 21:49:15 | 10200 | 291.47 | 0.118 | |
| 57603 | Jul 27 | 04:25:29 | 9000 | 291.74 | 0.104 | |
| 57604 | Jul 27 | 07:55:45 | 9000 | 291.88 | 0.104 | 5 |
| 57605 | Jul 27 | 10:53:48 | 9000 | 292.01 | 0.104 | |
| 57606 | Jul 27 | 18:39:52 | 9000 | 292.33 | 0.104 | |
| 57607 | Jul 27 | 21:49:31 | 9900 | 292.47 | 0.115 | |
| 57608 | Jul 28 | 04:19:07 | 9000 | 292.73 | 0.104 | |
| 57609 | Jul 28 | 07:15:50 | 9000 | 292.85 | 0.104 | |

TABLE 1—*Continued*

| Image (SWP Number) (1) | Observation Date (UT 1996) (2) | Start of Observation Time (UT hh:mm:ss) (3) | Exposure Time (s) (4) | JD (−2,450,000) (5) | Exposure Time (days) (6) | Notes[a] (7) |
|---|---|---|---|---|---|---|
| 57610..... | Jul 28 | 10:23:22 | 9000 | 292.98 | 0.104 | |
| 57611..... | Jul 28 | 18:36:04 | 9000 | 293.33 | 0.104 | |
| 57612..... | Jul 28 | 21:36:51 | 9000 | 293.45 | 0.104 | 8 |
| 57613..... | Jul 29 | 00:59:11 | 9000 | 293.59 | 0.104 | |
| 57614..... | Jul 29 | 04:14:46 | 9000 | 293.73 | 0.104 | |
| 57615..... | Jul 29 | 07:12:19 | 9000 | 293.85 | 0.104 | |
| 57616..... | Jul 29 | 10:10:10 | 9000 | 293.98 | 0.104 | |

[a] NOTES.—(1) Very noisy; short exposure time. (2) Source (partly) out of aperture. (3) Source probably partly out of aperture; short exposure time. (4) Short exposure time. (5) Large cosmic-ray blemish at He II. (6) Large cosmic-ray blemish at C IV. (7) Large cosmic-ray blemish in continuum redward of He II. (8) Large cosmic-ray blemish around 1875 Å.

With these results as a background, we decided to undertake an even more intensive monitoring program to attempt to measure both wavelength-dependent continuum phase differences and emission-line responses to continuum variations at the highest achievable time resolution for a sustained period during the final year of *IUE* operations. The original target for this investigation was the variable Seyfert 1 galaxy Mrk 335 (see, e.g., Kassebaum et al. 1997), but the outcome of a gyro failure in 1996 March limited target accessibility, and we therefore selected NGC 7469, also a known variable source (Salamanca, Alloin, & Pelat 1995, and references therein), as an alternative target for the campaign. We will present elsewhere results based on simultaneous monitoring with the *Rossi X-Ray Timing Explorer* (Nandra et al. 1997) and ground-based optical telescopes (Collier et al. 1997). Spectra obtained with the *Hubble Space Telescope (HST)* during this monitoring program will be discussed elsewhere (Kriss et al. 1997; Welsh et al. 1997).

In § 2, the observations are presented. Data analysis is described in § 3. The principal results are discussed in § 4, and a summary is given in § 5.

## 2. OBSERVATIONS

From 1996 June 10 to July 29, NGC 7469 was monitored continuously with *IUE*. The time interval between the midpoints of the last and the first spectrum was $48\overset{d}{.}84$, yielding 218 spectra, with an average sampling rate of one spectrum per $0\overset{d}{.}22$ (= 5.3 hr). Nearly all exposure times were 9000 s ($0\overset{d}{.}1$) long. All observations were made with the Short Wavelength Prime (SWP) camera (Harris & Sonneborn 1987) through the large aperture (10″ × 20″) of the short-wavelength spectrograph in the low-dispersion mode (resolution ∼6 Å; wavelength range 1150–1975 Å).

The log of the *IUE* observations is presented in Table 1. Column (1) presents the SWP image number of the observation; column (2), the UT date at the start of the observation; column (3), the UT time at the start of the observation; column (4), the exposure time in seconds; column (5), the Julian Date of the *middle* of the observation minus 2,450,000; and column (6), the exposure time in a fraction of a day. Finally, column (7) presents notes to the observations where appropriate. The 11 spectra marked with notes (1), (2), or (3) were deemed unsuitable and were excluded from any further analysis. The number of useful spectra was thus reduced to $N = 207$.

## 3. DATA ANALYSIS AND RESULTS

The raw images were reduced using both the standard NEWSIPS pipeline (Nichols et al. 1993) and the TOMSIPS reduction package (Ayres 1993). These routines produced very similar results, although the TOMSIPS-reduced data have somewhat smaller error bars and appear slightly smoother to the eye. We will compare the TOMSIPS and NEWSIPS results in the analyses, but generally they agree well with each other.

The TOMSIPS-reduced data had a slight nonlinear wavelength calibration error. (The low-dispersion TOMSIPS does not compensate for long-term secular drifts in the SWP wavelength scales, and the epoch of the original wavelength calibration [1985] is far removed from that of our observations of NGC 7469.) We corrected for this by fitting a second-order correction polynomial to the TOMSIPS wavelengths that aligned the peaks of the emission lines in the average TOMSIPS spectrum with the corresponding peaks in an *HST* spectrum of NGC 7469 taken on UT 1996 June 18 (Kriss et al. 1997). The wavelength calibration of the average NEWSIPS spectrum was found to be in good agreement with the *HST* spectrum, and no wavelength correction was applied. The spectra were then resampled onto a 1 Å pixel$^{-1}$ linear wavelength scale for easy comparison of the two data sets and for consistency in further analysis.

After the linearization of the average spectrum with an *HST* spectrum, small *zero-point* wavelength shifts between the spectra existed in both the TOMSIPS and NEWSIPS reduced data sets. These shifts generally were less than 1 Å but were as large as 2.5 Å in a few cases. They likely were due to small offsets of the target away from the center of the large aperture as a consequence of random pointing errors in the acquisition process. We compensated for the offsets by registering each spectrum to a common wavelength scale according to the apparent sharp peak of the C IV feature. We were able to measure its wavelength to a precision significantly better than 1 Å. This procedure resulted in a sharpening of the average spectrum, especially for the NEWSIPS data set, which indicated that the assumption of constancy of the C IV peak wavelength was justified.

The average wavelength of the Ly$\alpha$ and C IV peaks yields a redshift $z = 0.0165$ for NGC 7469, which is in good agreement with the value given in the NASA/IPAC Extragalactic Database (NED), $z = 0.0163$, and is identical to the [O III] $\lambda$5007 redshift found by Salamanca et al. (1995).

### 3.1. *Average and RMS Spectrum*

For both the TOMSIPS and NEWSIPS data sets, the average and root mean square (rms) spectra were calcu-

lated, where the average spectrum is defined by

$$\bar{s}(\lambda) = \frac{1}{N} \sum_{i=1}^{N} s_i(\lambda) , \quad (2)$$

and the rms spectrum $\sigma(\lambda)$ by

$$\sigma^2(\lambda) = \frac{1}{N-1} \sum_{i=1}^{N} [s_i(\lambda) - \bar{s}(\lambda)]^2 . \quad (3)$$

Here $s_i(\lambda)$ is the observed spectrum at time $t_i$ and $N = 207$ is the total number of useful spectra.

The average and rms spectra are shown in Figure 1, and the difference between the average TOMSIPS and the average NEWSIPS spectrum is shown in Figure 2. The difference spectrum shows the general consistency of the two methods, though there is a systematic discrepancy of up to 13% at the red end of the spectrum, i.e., the NEWSIPS fluxes are up to 13% higher than the TOMSIPS fluxes at wavelengths longward of ~1800 Å. Also, the NEWSIPS Lyα flux is systematically stronger than the TOMSIPS Lyα flux by ~15%. These systematic differences do not affect the results of this paper but may indicate a flux-calibration flaw in either TOMSIPS or NEWSIPS and is potentially important for those projects relying on accurate absolute fluxes.

The average spectrum is a measure of the constant component of the variable spectrum, and the rms spectrum is a measure of the variable component. From the average spectrum we can clearly discern the broad emission lines Lyα λ1216, N v λ1240, Si iv λ1400, C iv λ1549, He ii λ1640, and C iii] λ1909.

By comparing the strength of the emission lines and the continuum in the average and rms spectra, it can be seen

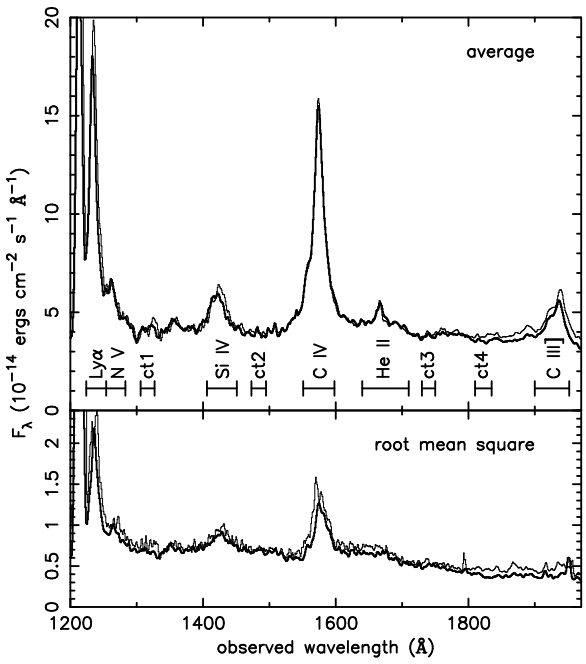


FIG. 1.—Average and rms *IUE* spectra of both the TOMSIPS (*thick line*) and NEWSIPS (*thin line*) data for the continuous monitoring campaign on NGC 7469 in 1996 June–July. The rms spectrum is the rms deviation from the mean spectrum. The wavelength intervals used for the calculation of the light curves of the four continuum bands and the emission lines are also marked. All wavelengths and fluxes are in the observer's frame.

that the line variations are much smaller than the continuum variations. Some lines do not vary at all, such as C iii], which is absent from the rms spectrum.

Also apparent from the rms spectrum is the slope in the continuum, which indicates that the continuum variations at the blue end of the spectrum are larger than those at the red end. This has been observed before in other AGNs (see, e.g., Edelson, Krolik, & Pike 1990).

### 3.2. *Continuum and Emission-Line Light Curves*

A more detailed impression of the variability of the continuum and emission-line fluxes can be obtained from the light curves.

The four continuum-flux light curves were determined as the unweighted average flux in the (observed) wave bands 1306–1327 Å, 1473–1495 Å, 1730–1750 Å, and 1805–1835 Å. The wave bands are marked "ct1" to "ct4," respectively, in Figure 1.

The emission-line light curves were determined by integrating all flux above a pseudocontinuum level, in the (observed) wave bands 1224–1254 Å for Lyα, 1255–1283 Å for N v, 1224–1283 Å for Lyα + N v, 1406–1451 Å for Si iv, 1551–1598 Å for C iv, 1640–1710 Å for He ii, and 1900–1952 Å for C iii]. The locations of these wave bands are shown in Figure 1. The pseudocontinuum was calculated by least-squares fitting of a power law to all pixels in the four continuum wave bands defined before. As a check of this procedure, we also derived emission-line fluxes by subtracting a pseudocontinuum, which was defined as a straight-line fit to the continuum level on each side of each emission line. This gave consistent results with the procedure adopted here.

Though the C iv line clearly extends beyond the tight wavelength limits defined here, the rms spectrum (Fig. 1) shows there is no significant variability in the outer parts of the C iv emission line. In order to keep the signal-to-noise ratio as high as possible, we integrate the line flux only over the most *variable* part of the line. The rms spectrum was also used to define the wavelength integration limits of the other lines. However, the width of the He ii line and its low contrast to the continuum make it difficult to define its limits in the rms spectrum; therefore, we use the average spectrum to define its limits. Because the C iii] line is not variable and thus not visible at all in the rms spectrum, we also use the average spectrum for its limits.

The error bars of the emission-line fluxes are not straightforward to calculate because a pseudocontinuum, with uncertain error, is subtracted before integrating over the emission line. We have adopted a conservative approach in this respect and estimate both the continuum and emission-line flux errors by assuming there is no intrinsic variation between two consecutive measurements. We then calculate the rms of the distribution of the flux ratios $F_{i+1}/F_i$ and compare this to the mean observed uncertainty as directly derived from the spectra. We then scale the latter such that the rms of the flux ratios equals the mean observed uncertainty (Rodríguez-Pascual et al. 1997). This procedure produces an upper limit to the size of the error bars because in reality, the assumption of nonvariability between consecutive observations is not entirely valid.

The TOMSIPS- and NEWSIPS-derived light curves are very similar, although the TOMSIPS data have somewhat smaller error bars associated with the fluxes. The TOMSIPS fluxes of the C iii] line and the continuum at

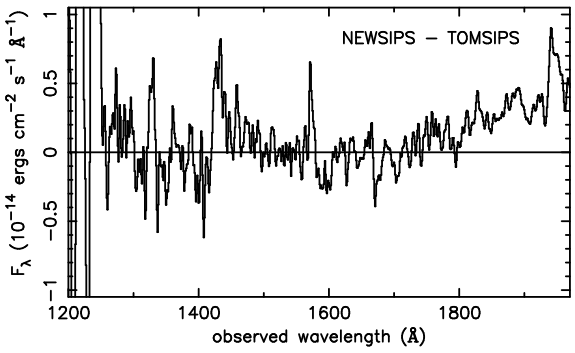


FIG. 2.—Difference between the average TOMSIPS and average NEWSIPS spectrum of NGC 7469.

1825 Å are systematically ~10% lower than the NEWSIPS fluxes, as are the TOMSIPS Lyα and N v fluxes. For conciseness, we tabulate only the TOMSIPS light curves in Tables 2 and 3, but we show both NEWSIPS and TOMSIPS light curves in Figures 3 and 4, respectively. All fluxes are in the observer's frame.

The continuum light curves clearly show several "events," each with a duration of 10–15 days. The amplitude of these variations decreases in the longer wavelength continuum light curves, as was already evident from the slope of the rms spectrum.

All emission-line fluxes are observed to possess a slow, downward trend from the beginning to the end of the campaign. The decrease in average line flux between the beginning of the campaign and the end of the campaign is quite large: ~30% for Lyα, ~40% for Si IV, ~25% for C IV, and ~30% for He II. These trends are possibly in response to low-frequency continuum variability to which the present intensive monitoring campaign is not sensitive.

Apart from the decreasing trends in the line fluxes, the "events" in the continuum light curves can be weakly seen in the Lyα, N V, Si IV, C IV, and possibly He II light curves, albeit with short time delays with respect to the continuum. For example, both Lyα and C IV reach local maxima around Julian Dates 267 and 278, approximately 2-3 days after the continua reach their local maxima. We will quantify this later by means of a cross-correlation analysis.

### 3.3. *Variability Characteristics*

We can characterize the continuum and line variability by means of several parameters. The first two parameters are straightforward, namely the mean flux $\bar{F}$ and the rms flux $\sigma_F$ defined in the usual manner:

$$\bar{F} = \frac{1}{N}\sum_{i=1}^{N} F_i \quad \text{and} \quad \sigma_F^2 = \frac{1}{N-1}\sum_{i=1}^{N}(F_i - \bar{F})^2 \,. \quad (4)$$

Another useful parameter is the ratio of the maximum to the minimum flux, $R_{\max}$, though for some of the emission lines, notably He II and C III], where the random errors are comparable to the amplitude of the intrinsic variations, this parameter is dominated by noise and is therefore not very meaningful.

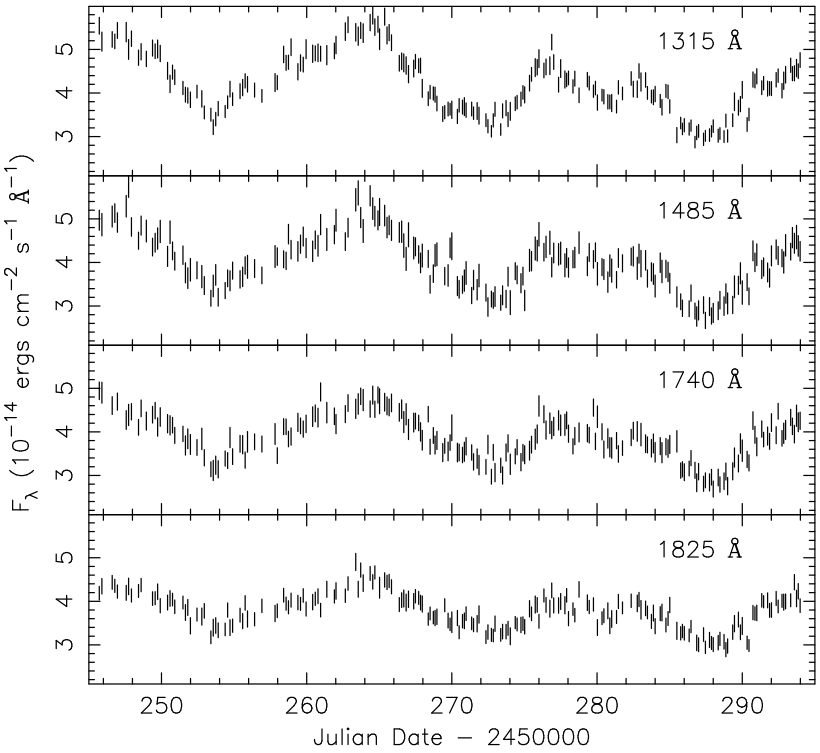


FIG. 3*a*

FIG. 3.—The continuum (*a*) and emission-line (*b*) flux light curves of the NGC 7469 NEWSIPS-reduced data and the 1 $\sigma$ errors

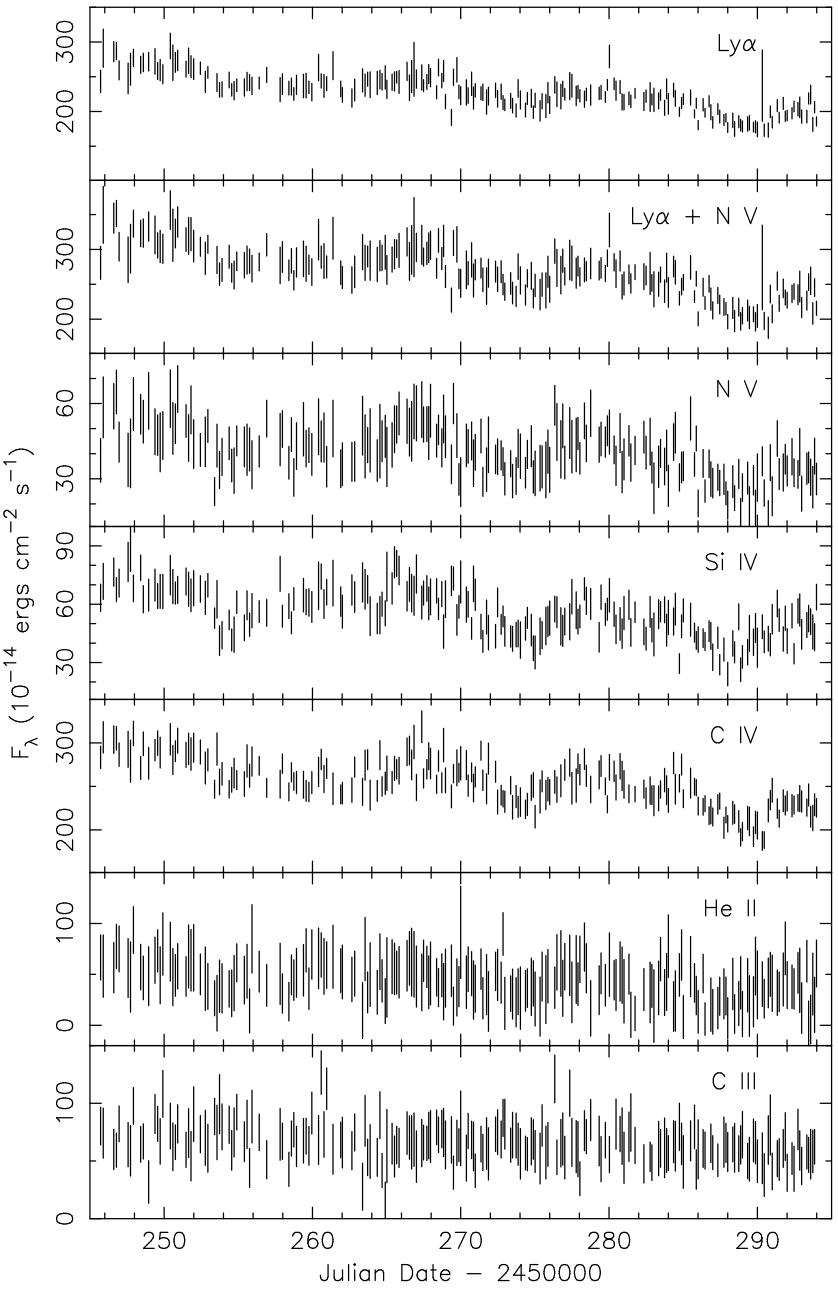


FIG. 3*b*

A fourth parameter, $F_{\rm var}$, is an estimate of the amplitude of the intrinsic variability relative to the mean flux, corrected for the measurement errors $\epsilon_i$, and is defined as

$$F_{\rm var} = \frac{1}{\bar{F}} \sqrt{(\sigma_F^2 - \Delta^2)}\,, \tag{5}$$

where $\Delta^2$ is the mean square value of the measurement uncertainties, i.e.,

$$\Delta^2 = \frac{1}{N} \sum_{i=1}^{N} \epsilon_i^2\,. \tag{6}$$

The four variability parameters are tabulated for each light curve in Table 4 for both the TOMSIPS ("T") and the NEWSIPS ("N") data. The differences between the TOMSIPS and NEWSIPS results provide an estimate of the uncertainty in these parameters. As expected, $R_{\rm max}$ is uncertain for the He II and C III] emission lines owing to stochastic errors in the data that are larger than the intrinsic variability. The parameter $F_{\rm var}$ is also uncertain for these lines, where $\Delta^2$ can be larger than $\sigma_F^2$; this is due to the conservative error estimates adopted here.

Parameter $F_{\rm var}$ decreases in the continuum toward longer wavelengths, again indicating that the amplitude of the variations decreases with increasing wavelength. Note that for the emission lines, $F_{\rm var}$ is relatively large owing to the trend in the data, which increases the value of $\sigma_F^2$. For the emission lines, therefore, $F_{\rm var}$ overestimates the strength of the fast intrinsic variations.

Columns (2) and (3) of Table 4 show the number of useful data points $N_{\rm data}$ in the light curves. Any difference between

TABLE 2

CONTINUUM FLUXES (TOMSIPS)

| JD (−2,450,000) (1) | $F_\lambda$(1315 Å) (2) | $F_\lambda$(1485 Å) (3) | $F_\lambda$(1740 Å) (4) | $F_\lambda$(1825 Å) (5) |
|---|---|---|---|---|
| 245.72 ..... | 5.39 ± 0.15 | 4.77 ± 0.20 | 4.84 ± 0.16 | 3.96 ± 0.13 |
| 245.90 ..... | 5.31 ± 0.17 | 4.91 ± 0.21 | 4.56 ± 0.17 | 4.15 ± 0.14 |
| 246.61 ..... | 5.31 ± 0.15 | 4.92 ± 0.20 | 4.57 ± 0.16 | 4.04 ± 0.13 |
| 246.79 ..... | 5.25 ± 0.17 | 5.06 ± 0.21 | 4.88 ± 0.17 | 4.07 ± 0.14 |
| 246.97 ..... | 5.42 ± 0.18 | 4.79 ± 0.23 | 4.45 ± 0.19 | 4.08 ± 0.15 |
| 247.57 ..... | 5.33 ± 0.17 | 5.08 ± 0.21 | 4.10 ± 0.17 | 3.95 ± 0.14 |
| 247.74 ..... | 5.30 ± 0.17 | 5.68 ± 0.21 | 4.27 ± 0.17 | 4.01 ± 0.14 |
| 247.93 ..... | 5.12 ± 0.17 | 4.79 ± 0.21 | 4.39 ± 0.17 | 3.85 ± 0.14 |
| 248.42 ..... | 4.97 ± 0.15 | 4.28 ± 0.20 | 4.09 ± 0.16 | 3.98 ± 0.13 |
| 248.60 ..... | 4.86 ± 0.14 | 4.89 ± 0.19 | 4.48 ± 0.15 | 4.03 ± 0.12 |
| 248.96 ..... | 4.76 ± 0.15 | 4.43 ± 0.21 | 4.18 ± 0.16 | 3.97 ± 0.13 |
| 249.39 ..... | 4.99 ± 0.15 | 4.21 ± 0.20 | 4.24 ± 0.16 | 3.92 ± 0.13 |
| 249.57 ..... | 4.71 ± 0.17 | 4.59 ± 0.21 | 4.29 ± 0.17 | 3.79 ± 0.14 |
| 249.74 ..... | 4.89 ± 0.18 | 4.66 ± 0.24 | 4.06 ± 0.19 | 4.01 ± 0.15 |
| 249.92 ..... | 4.68 ± 0.15 | 4.53 ± 0.21 | 4.23 ± 0.16 | 3.74 ± 0.13 |
| 250.42 ..... | 4.50 ± 0.15 | 4.19 ± 0.20 | 4.14 ± 0.16 | 3.80 ± 0.13 |
| 250.59 ..... | 4.19 ± 0.17 | 4.25 ± 0.22 | 4.09 ± 0.17 | 3.69 ± 0.14 |
| 250.76 ..... | 4.33 ± 0.15 | 4.12 ± 0.20 | 3.88 ± 0.16 | 3.69 ± 0.13 |
| 250.92 ..... | 4.37 ± 0.15 | 4.03 ± 0.20 | 3.88 ± 0.16 | 3.60 ± 0.13 |
| 251.48 ..... | 3.90 ± 0.14 | ... | 3.74 ± 0.15 | 3.64 ± 0.12 |
| 251.65 ..... | 3.98 ± 0.18 | 3.73 ± 0.23 | 3.67 ± 0.19 | 3.44 ± 0.15 |
| 251.81 ..... | 3.94 ± 0.15 | 3.69 ± 0.19 | 3.77 ± 0.16 | 3.56 ± 0.13 |
| 251.99 ..... | 3.77 ± 0.18 | 3.67 ± 0.22 | 3.55 ± 0.19 | 3.29 ± 0.15 |
| 252.45 ..... | 3.94 ± 0.13 | 3.62 ± 0.17 | 3.48 ± 0.13 | 3.57 ± 0.11 |
| 252.78 ..... | 3.86 ± 0.14 | 3.53 ± 0.17 | 3.66 ± 0.15 | 3.38 ± 0.12 |
| 252.95 ..... | 3.63 ± 0.14 | 3.28 ± 0.19 | 3.45 ± 0.15 | 3.45 ± 0.12 |
| 253.40 ..... | 3.33 ± 0.13 | 2.91 ± 0.17 | 3.09 ± 0.13 | 2.82 ± 0.11 |
| 253.57 ..... | 3.21 ± 0.14 | 3.20 ± 0.17 | 3.07 ± 0.15 | 3.03 ± 0.12 |
| 253.74 ..... | 3.44 ± 0.14 | 3.37 ± 0.17 | 3.19 ± 0.15 | 3.19 ± 0.12 |
| 253.91 ..... | 3.59 ± 0.13 | 2.96 ± 0.17 | 3.15 ± 0.13 | 3.12 ± 0.11 |
| 254.39 ..... | 3.50 ± 0.13 | 3.06 ± 0.16 | 3.28 ± 0.13 | 3.09 ± 0.11 |
| 254.56 ..... | 3.74 ± 0.13 | 3.44 ± 0.17 | 3.38 ± 0.13 | 3.42 ± 0.11 |
| 254.72 ..... | 4.13 ± 0.15 | 3.48 ± 0.19 | 3.62 ± 0.16 | 3.19 ± 0.13 |
| 254.90 ..... | 3.79 ± 0.13 | 3.63 ± 0.17 | 3.47 ± 0.13 | 3.23 ± 0.11 |
| 255.41 ..... | 4.05 ± 0.17 | 3.74 ± 0.24 | 3.80 ± 0.20 | 3.42 ± 0.14 |
| 255.59 ..... | 4.12 ± 0.18 | 3.64 ± 0.23 | 3.73 ± 0.19 | 3.37 ± 0.15 |
| 255.76 ..... | 4.32 ± 0.15 | 3.95 ± 0.21 | 3.55 ± 0.16 | 3.44 ± 0.13 |
| 255.93 ..... | 3.98 ± 0.17 | 3.65 ± 0.22 | 3.67 ± 0.17 | 3.35 ± 0.14 |
| 256.41 ..... | 4.06 ± 0.15 | 3.76 ± 0.20 | 3.47 ± 0.16 | 3.35 ± 0.13 |
| 256.92 ..... | 3.99 ± 0.14 | 3.54 ± 0.17 | 3.56 ± 0.15 | 3.65 ± 0.12 |
| 257.82 ..... | 4.36 ± 0.14 | 3.94 ± 0.19 | 3.80 ± 0.15 | 3.48 ± 0.12 |
| 257.98 ..... | 4.28 ± 0.15 | 4.07 ± 0.20 | 3.53 ± 0.16 | 3.51 ± 0.13 |
| 258.41 ..... | 4.70 ± 0.15 | 4.02 ± 0.20 | 3.88 ± 0.16 | 3.75 ± 0.13 |
| 258.58 ..... | 4.47 ± 0.15 | 4.18 ± 0.20 | 3.95 ± 0.16 | 3.74 ± 0.13 |
| 258.75 ..... | 4.59 ± 0.15 | 4.41 ± 0.20 | 3.76 ± 0.16 | 3.62 ± 0.13 |
| 258.93 ..... | 4.89 ± 0.14 | 4.31 ± 0.19 | 3.82 ± 0.15 | 3.74 ± 0.12 |
| 259.40 ..... | 4.57 ± 0.14 | 4.17 ± 0.19 | 4.04 ± 0.15 | 3.69 ± 0.12 |
| 259.58 ..... | 4.67 ± 0.14 | 4.43 ± 0.19 | 3.95 ± 0.15 | 3.70 ± 0.12 |
| 259.76 ..... | 4.58 ± 0.18 | 4.45 ± 0.23 | 3.90 ± 0.19 | 3.81 ± 0.15 |
| 259.96 ..... | 4.82 ± 0.17 | 4.58 ± 0.21 | 4.29 ± 0.17 | 3.75 ± 0.14 |
| 260.41 ..... | 4.85 ± 0.17 | 4.18 ± 0.21 | 4.13 ± 0.17 | 3.76 ± 0.14 |
| 260.59 ..... | 4.86 ± 0.17 | 4.31 ± 0.21 | 4.27 ± 0.17 | 3.74 ± 0.14 |
| 260.78 ..... | 5.02 ± 0.19 | 4.22 ± 0.24 | 4.22 ± 0.20 | 3.82 ± 0.16 |
| 260.96 ..... | 4.90 ± 0.18 | 4.68 ± 0.23 | 4.70 ± 0.19 | 3.62 ± 0.15 |
| 261.39 ..... | 4.86 ± 0.14 | 4.51 ± 0.19 | 4.17 ± 0.15 | 3.89 ± 0.12 |
| 261.91 ..... | 4.88 ± 0.14 | 4.49 ± 0.19 | 4.24 ± 0.15 | 3.88 ± 0.12 |
| 262.02 ..... | 5.06 ± 0.17 | 4.53 ± 0.22 | 4.00 ± 0.17 | 4.03 ± 0.14 |
| 262.66 ..... | 5.17 ± 0.15 | 4.69 ± 0.20 | 4.32 ± 0.16 | 3.94 ± 0.13 |
| 262.85 ..... | 5.36 ± 0.14 | 4.80 ± 0.19 | 4.49 ± 0.16 | 4.10 ± 0.13 |
| 263.38 ..... | 5.50 ± 0.17 | 5.00 ± 0.21 | 4.48 ± 0.17 | 4.17 ± 0.14 |
| 263.55 ..... | 5.26 ± 0.17 | 5.37 ± 0.21 | 4.35 ± 0.17 | 4.15 ± 0.14 |
| 263.72 ..... | 5.33 ± 0.18 | 4.78 ± 0.23 | 4.59 ± 0.19 | 4.12 ± 0.15 |
| 263.89 ..... | 5.13 ± 0.15 | 4.63 ± 0.20 | 4.51 ± 0.16 | 4.08 ± 0.13 |
| 264.37 ..... | 5.55 ± 0.14 | 5.40 ± 0.19 | 4.39 ± 0.15 | 4.17 ± 0.12 |
| 264.55 ..... | 5.67 ± 0.19 | 5.01 ± 0.24 | 4.51 ± 0.20 | 4.12 ± 0.16 |
| 264.70 ..... | 5.53 ± 0.15 | 4.97 ± 0.19 | 4.49 ± 0.16 | 4.24 ± 0.13 |
| 264.91 ..... | 5.76 ± 0.15 | 4.97 ± 0.19 | 4.70 ± 0.16 | 4.42 ± 0.13 |
| 265.02 ..... | 4.97 ± 0.23 | 4.92 ± 0.29 | 4.67 ± 0.24 | 3.80 ± 0.19 |
| 265.37 ..... | 5.61 ± 0.18 | 4.91 ± 0.23 | 4.53 ± 0.19 | 4.11 ± 0.15 |
| 265.53 ..... | 5.26 ± 0.17 | 4.65 ± 0.21 | 4.50 ± 0.17 | 4.08 ± 0.14 |
| 265.68 ..... | 5.26 ± 0.19 | 4.85 ± 0.24 | 4.33 ± 0.20 | 4.02 ± 0.16 |
| 265.84 ..... | 5.12 ± 0.19 | 4.74 ± 0.24 | 4.59 ± 0.20 | 4.06 ± 0.16 |

TABLE 2—*Continued*

| JD (−2,450,000) (1) | $F_\lambda$(1315 Å) (2) | $F_\lambda$(1485 Å) (3) | $F_\lambda$(1740 Å) (4) | $F_\lambda$(1825 Å) (5) |
|---|---|---|---|---|
| 266.38 ..... | 4.45 ± 0.14 | 4.47 ± 0.19 | 3.89 ± 0.15 | 3.49 ± 0.12 |
| 266.54 ..... | 4.75 ± 0.15 | 4.61 ± 0.19 | 4.32 ± 0.16 | 3.76 ± 0.13 |
| 266.69 ..... | 4.65 ± 0.15 | 4.36 ± 0.20 | 4.14 ± 0.16 | 3.83 ± 0.13 |
| 266.85 ..... | 4.58 ± 0.19 | 3.99 ± 0.24 | 4.24 ± 0.20 | 3.65 ± 0.16 |
| 267.01 ..... | 4.53 ± 0.15 | 4.44 ± 0.20 | 3.92 ± 0.16 | 3.81 ± 0.13 |
| 267.37 ..... | 4.51 ± 0.14 | 4.10 ± 0.19 | 4.05 ± 0.15 | 3.73 ± 0.12 |
| 267.49 ..... | 4.55 ± 0.15 | 4.41 ± 0.20 | 4.16 ± 0.16 | 3.84 ± 0.13 |
| 267.71 ..... | 4.65 ± 0.17 | 4.13 ± 0.22 | 4.05 ± 0.17 | 3.87 ± 0.14 |
| 267.84 ..... | 4.64 ± 0.18 | 4.15 ± 0.23 | 3.96 ± 0.19 | 3.75 ± 0.15 |
| 267.96 ..... | 4.32 ± 0.17 | 4.34 ± 0.21 | 3.81 ± 0.17 | 3.79 ± 0.14 |
| 268.37 ..... | 4.07 ± 0.17 | 3.76 ± 0.21 | 3.91 ± 0.17 | 3.56 ± 0.14 |
| 268.50 ..... | 4.13 ± 0.15 | 3.72 ± 0.20 | 3.85 ± 0.16 | 3.41 ± 0.13 |
| 268.72 ..... | 4.04 ± 0.14 | 3.72 ± 0.17 | 3.79 ± 0.15 | 3.52 ± 0.12 |
| 268.84 ..... | 3.92 ± 0.17 | 3.92 ± 0.22 | 3.73 ± 0.17 | 3.42 ± 0.14 |
| 268.97 ..... | 3.72 ± 0.17 | 3.90 ± 0.21 | 3.66 ± 0.17 | 3.25 ± 0.14 |
| 269.37 ..... | 3.67 ± 0.14 | 3.04 ± 0.19 | 3.32 ± 0.15 | 3.03 ± 0.12 |
| 269.51 ..... | 3.72 ± 0.14 | 3.50 ± 0.17 | 3.68 ± 0.15 | 3.42 ± 0.12 |
| 269.74 ..... | 3.81 ± 0.13 | 3.52 ± 0.16 | 3.60 ± 0.13 | 3.31 ± 0.11 |
| 269.88 ..... | 3.62 ± 0.17 | 3.87 ± 0.22 | 3.62 ± 0.17 | 3.12 ± 0.14 |
| 270.00 ..... | 3.59 ± 0.23 | 4.32 ± 0.29 | 3.77 ± 0.24 | 3.28 ± 0.19 |
| 270.38 ..... | 3.62 ± 0.13 | 3.24 ± 0.16 | 3.40 ± 0.13 | 3.33 ± 0.11 |
| 270.50 ..... | 3.77 ± 0.15 | 3.30 ± 0.20 | 3.32 ± 0.16 | 3.26 ± 0.13 |
| 270.73 ..... | 3.79 ± 0.14 | 3.44 ± 0.17 | 3.45 ± 0.15 | 3.26 ± 0.12 |
| 270.86 ..... | 3.69 ± 0.14 | 3.44 ± 0.17 | 3.40 ± 0.15 | 3.31 ± 0.12 |
| 270.98 ..... | 3.51 ± 0.18 | 3.35 ± 0.23 | 3.48 ± 0.19 | 3.35 ± 0.15 |
| 271.36 ..... | 3.67 ± 0.15 | 3.29 ± 0.20 | 3.38 ± 0.16 | 3.28 ± 0.13 |
| 271.49 ..... | 3.74 ± 0.13 | 3.46 ± 0.17 | 3.36 ± 0.13 | 3.27 ± 0.11 |
| 271.74 ..... | 3.55 ± 0.14 | 3.19 ± 0.17 | 3.41 ± 0.15 | 3.26 ± 0.12 |
| 271.87 ..... | 3.56 ± 0.17 | 3.30 ± 0.22 | 3.24 ± 0.17 | 3.16 ± 0.14 |
| 272.35 ..... | 3.54 ± 0.13 | 3.03 ± 0.17 | 3.13 ± 0.13 | 3.00 ± 0.11 |
| 272.48 ..... | 3.31 ± 0.17 | 2.76 ± 0.21 | 3.16 ± 0.17 | 3.12 ± 0.14 |
| 272.72 ..... | 3.34 ± 0.15 | 3.04 ± 0.20 | 3.03 ± 0.16 | 3.04 ± 0.13 |
| 272.85 ..... | 3.40 ± 0.14 | 2.95 ± 0.19 | 3.26 ± 0.15 | 3.04 ± 0.12 |
| 272.97 ..... | 3.43 ± 0.14 | 2.94 ± 0.19 | 3.05 ± 0.15 | 3.21 ± 0.12 |
| 273.36 ..... | 3.17 ± 0.13 | 3.08 ± 0.16 | 3.10 ± 0.13 | 2.93 ± 0.11 |
| 273.49 ..... | 3.53 ± 0.15 | 3.15 ± 0.20 | 2.95 ± 0.16 | 2.91 ± 0.13 |
| 273.73 ..... | 3.66 ± 0.14 | 3.12 ± 0.17 | 3.42 ± 0.15 | 3.11 ± 0.12 |
| 273.87 ..... | 3.53 ± 0.14 | 3.22 ± 0.17 | 3.33 ± 0.15 | 3.21 ± 0.12 |
| 274.02 ..... | 3.67 ± 0.18 | 3.12 ± 0.22 | 3.38 ± 0.19 | 3.10 ± 0.15 |
| 274.36 ..... | 3.87 ± 0.11 | 3.51 ± 0.15 | 3.30 ± 0.13 | 3.27 ± 0.11 |
| 274.49 ..... | 3.89 ± 0.17 | 3.59 ± 0.22 | 3.48 ± 0.17 | 3.22 ± 0.14 |
| 274.76 ..... | 3.93 ± 0.14 | 3.67 ± 0.17 | 3.42 ± 0.15 | 3.35 ± 0.12 |
| 274.89 ..... | 3.92 ± 0.14 | 3.51 ± 0.19 | 3.51 ± 0.15 | 3.34 ± 0.12 |
| 275.01 ..... | 4.17 ± 0.18 | 3.26 ± 0.22 | 3.48 ± 0.19 | 3.37 ± 0.15 |
| 275.35 ..... | 4.32 ± 0.14 | 3.98 ± 0.17 | 3.63 ± 0.15 | 3.48 ± 0.12 |
| 275.48 ..... | 4.35 ± 0.14 | 3.68 ± 0.17 | 3.71 ± 0.15 | 3.48 ± 0.12 |
| 275.74 ..... | 4.66 ± 0.14 | 4.35 ± 0.19 | 3.74 ± 0.15 | 3.69 ± 0.12 |
| 275.88 ..... | 4.60 ± 0.15 | 4.27 ± 0.20 | 3.91 ± 0.16 | 3.70 ± 0.13 |
| 276.00 ..... | 4.92 ± 0.20 | 4.65 ± 0.26 | 4.13 ± 0.21 | 3.58 ± 0.17 |
| 276.34 ..... | 4.78 ± 0.15 | 4.10 ± 0.20 | 4.22 ± 0.16 | 3.92 ± 0.13 |
| 276.48 ..... | 4.65 ± 0.14 | 4.39 ± 0.19 | 4.06 ± 0.15 | 3.68 ± 0.12 |
| 276.75 ..... | 4.71 ± 0.17 | 4.42 ± 0.21 | 4.03 ± 0.17 | 3.61 ± 0.14 |
| 276.88 ..... | 5.10 ± 0.15 | 4.05 ± 0.20 | 4.18 ± 0.16 | 3.87 ± 0.13 |
| 277.01 ..... | 4.64 ± 0.17 | 4.10 ± 0.22 | 4.05 ± 0.17 | 3.61 ± 0.14 |
| 277.35 ..... | 4.48 ± 0.15 | 4.20 ± 0.20 | 3.98 ± 0.16 | 3.71 ± 0.13 |
| 277.49 ..... | 4.60 ± 0.18 | 4.32 ± 0.23 | 4.11 ± 0.19 | 3.77 ± 0.15 |
| 277.78 ..... | 4.24 ± 0.14 | 3.96 ± 0.19 | 3.94 ± 0.15 | 3.69 ± 0.12 |
| 277.90 ..... | 4.32 ± 0.18 | 4.05 ± 0.24 | 3.99 ± 0.19 | 3.80 ± 0.15 |
| 278.03 ..... | 4.41 ± 0.19 | 4.07 ± 0.25 | 3.88 ± 0.20 | 3.47 ± 0.16 |
| 278.34 ..... | 4.35 ± 0.15 | 4.04 ± 0.20 | 3.70 ± 0.16 | 3.67 ± 0.13 |
| 278.47 ..... | 4.54 ± 0.15 | 4.13 ± 0.20 | 3.94 ± 0.16 | 3.54 ± 0.13 |
| 278.76 ..... | 4.26 ± 0.15 | 4.11 ± 0.20 | 3.95 ± 0.16 | 4.02 ± 0.13 |
| 279.33 ..... | 4.36 ± 0.17 | 3.91 ± 0.21 | 3.90 ± 0.17 | 3.54 ± 0.14 |
| 279.46 ..... | 4.04 ± 0.14 | 3.95 ± 0.17 | 3.82 ± 0.15 | 3.53 ± 0.12 |
| 279.75 ..... | 3.99 ± 0.15 | 3.89 ± 0.20 | 4.03 ± 0.16 | 3.90 ± 0.13 |
| 279.89 ..... | 4.10 ± 0.14 | 3.75 ± 0.19 | 3.74 ± 0.15 | 3.80 ± 0.12 |
| 280.02 ..... | 3.93 ± 0.15 | 3.84 ± 0.21 | 4.48 ± 0.16 | 3.52 ± 0.13 |
| 280.34 ..... | 4.05 ± 0.14 | 3.94 ± 0.17 | 4.65 ± 0.15 | 3.48 ± 0.12 |
| 280.47 ..... | 3.88 ± 0.14 | 3.71 ± 0.19 | 3.52 ± 0.15 | 3.46 ± 0.12 |
| 280.74 ..... | 3.91 ± 0.15 | 3.78 ± 0.20 | 3.72 ± 0.16 | 3.60 ± 0.13 |
| 280.88 ..... | 3.83 ± 0.15 | 3.82 ± 0.20 | 3.52 ± 0.16 | 3.23 ± 0.13 |
| 281.01 ..... | 3.69 ± 0.17 | 3.49 ± 0.21 | 3.45 ± 0.17 | 3.37 ± 0.14 |

TABLE 2—*Continued*

| JD (−2,450,000) (1) | $F_\lambda$(1315 Å) (2) | $F_\lambda$(1485 Å) (3) | $F_\lambda$(1740 Å) (4) | $F_\lambda$(1825 Å) (5) |
|---|---|---|---|---|
| 281.34 ..... | 3.76 ± 0.14 | 3.71 ± 0.17 | 3.46 ± 0.15 | 3.41 ± 0.12 |
| 281.47 ..... | 4.07 ± 0.13 | 3.67 ± 0.16 | 3.60 ± 0.13 | 3.52 ± 0.11 |
| 281.75 ..... | 4.23 ± 0.13 | 3.89 ± 0.16 | 3.59 ± 0.13 | 3.63 ± 0.11 |
| 282.35 ..... | 4.41 ± 0.15 | 4.13 ± 0.20 | 3.78 ± 0.16 | 3.95 ± 0.13 |
| 282.49 ..... | 4.22 ± 0.15 | 3.91 ± 0.20 | 3.94 ± 0.16 | 4.31 ± 0.13 |
| 282.77 ..... | 4.22 ± 0.14 | 3.68 ± 0.19 | 3.78 ± 0.15 | 3.76 ± 0.12 |
| 282.89 ..... | ... | 3.84 ± 0.19 | 4.36 ± 0.15 | 3.87 ± 0.12 |
| 283.02 ..... | 4.31 ± 0.17 | 3.69 ± 0.22 | 3.88 ± 0.17 | 3.64 ± 0.14 |
| 283.34 ..... | 4.33 ± 0.14 | 3.82 ± 0.17 | 3.77 ± 0.15 | 3.63 ± 0.12 |
| 283.47 ..... | 4.11 ± 0.15 | 3.51 ± 0.20 | 3.68 ± 0.16 | 3.56 ± 0.13 |
| 283.74 ..... | 4.00 ± 0.15 | 3.67 ± 0.20 | 3.63 ± 0.16 | 3.41 ± 0.13 |
| 283.88 ..... | 4.08 ± 0.14 | 3.76 ± 0.19 | 3.55 ± 0.15 | 3.55 ± 0.12 |
| 284.00 ..... | 4.08 ± 0.15 | 3.68 ± 0.19 | 3.56 ± 0.16 | 3.31 ± 0.13 |
| 284.35 ..... | 3.88 ± 0.15 | 3.80 ± 0.20 | 3.53 ± 0.16 | 3.46 ± 0.13 |
| 284.47 ..... | 3.83 ± 0.14 | 3.53 ± 0.19 | 3.43 ± 0.15 | 3.48 ± 0.12 |
| 284.74 ..... | 3.92 ± 0.15 | 3.68 ± 0.20 | 3.54 ± 0.16 | 3.27 ± 0.13 |
| 284.89 ..... | 4.00 ± 0.14 | 3.48 ± 0.17 | 3.52 ± 0.15 | 3.36 ± 0.12 |
| 285.01 ..... | 3.68 ± 0.18 | 3.36 ± 0.23 | 3.36 ± 0.19 | 3.51 ± 0.15 |
| 285.49 ..... | 3.14 ± 0.20 | 2.98 ± 0.25 | 3.52 ± 0.21 | 3.14 ± 0.17 |
| 285.76 ..... | 3.25 ± 0.13 | 2.91 ± 0.16 | 2.96 ± 0.13 | 3.04 ± 0.11 |
| 285.88 ..... | 3.07 ± 0.15 | 2.83 ± 0.19 | 3.18 ± 0.16 | 3.05 ± 0.13 |
| 286.01 ..... | 3.30 ± 0.17 | 3.33 ± 0.22 | 3.10 ± 0.17 | 2.95 ± 0.14 |
| 286.34 ..... | 3.16 ± 0.15 | 2.74 ± 0.21 | 3.19 ± 0.17 | 3.04 ± 0.13 |
| 286.47 ..... | 3.28 ± 0.13 | 3.03 ± 0.16 | 3.10 ± 0.13 | 2.95 ± 0.11 |
| 286.74 ..... | 2.85 ± 0.17 | 2.61 ± 0.21 | 3.09 ± 0.17 | ... |
| 286.86 ..... | 3.02 ± 0.13 | 2.49 ± 0.17 | 2.94 ± 0.13 | 2.95 ± 0.12 |
| 286.99 ..... | 3.24 ± 0.14 | 2.91 ± 0.17 | 2.92 ± 0.15 | 2.95 ± 0.12 |
| 287.33 ..... | 3.01 ± 0.13 | 3.02 ± 0.16 | 2.94 ± 0.13 | 3.06 ± 0.11 |
| 287.46 ..... | 3.06 ± 0.13 | 2.79 ± 0.15 | 3.09 ± 0.13 | 2.83 ± 0.11 |
| 287.74 ..... | 3.03 ± 0.14 | 2.84 ± 0.19 | 2.83 ± 0.16 | 2.92 ± 0.13 |
| 287.88 ..... | 3.04 ± 0.17 | 2.89 ± 0.21 | 2.97 ± 0.17 | 3.01 ± 0.14 |
| 288.00 ..... | 3.30 ± 0.14 | 2.77 ± 0.19 | 2.85 ± 0.15 | 2.84 ± 0.12 |
| 288.34 ..... | 3.05 ± 0.15 | 2.73 ± 0.19 | 2.84 ± 0.16 | 2.89 ± 0.13 |
| 288.46 ..... | 3.30 ± 0.14 | 3.14 ± 0.19 | 2.89 ± 0.15 | 2.93 ± 0.12 |
| 288.74 ..... | 3.05 ± 0.13 | 2.93 ± 0.17 | 2.91 ± 0.13 | 2.91 ± 0.11 |
| 288.87 ..... | 3.36 ± 0.14 | 3.01 ± 0.17 | 3.11 ± 0.15 | 2.74 ± 0.12 |
| 288.99 ..... | 3.14 ± 0.15 | 2.92 ± 0.20 | 2.99 ± 0.16 | 2.82 ± 0.13 |
| 289.34 ..... | 3.46 ± 0.13 | 3.03 ± 0.16 | 3.14 ± 0.13 | 3.18 ± 0.11 |
| 289.46 ..... | 3.70 ± 0.13 | 3.11 ± 0.16 | 3.38 ± 0.13 | 3.17 ± 0.11 |
| 289.73 ..... | 3.60 ± 0.14 | 3.43 ± 0.19 | 3.51 ± 0.15 | 3.39 ± 0.12 |
| 289.87 ..... | 3.88 ± 0.15 | 3.44 ± 0.20 | 3.48 ± 0.16 | 3.31 ± 0.13 |
| 290.00 ..... | 3.93 ± 0.14 | 3.44 ± 0.19 | 3.43 ± 0.15 | 3.35 ± 0.12 |
| 290.33 ..... | 3.51 ± 0.15 | 3.41 ± 0.20 | 3.27 ± 0.16 | 2.95 ± 0.13 |
| 290.46 ..... | 3.56 ± 0.13 | 3.19 ± 0.16 | 3.02 ± 0.13 | 2.96 ± 0.11 |
| 290.73 ..... | 4.36 ± 0.17 | 4.11 ± 0.21 | 4.09 ± 0.17 | 3.52 ± 0.14 |
| 290.87 ..... | 4.32 ± 0.18 | 4.06 ± 0.23 | 3.71 ± 0.19 | 3.61 ± 0.15 |
| 291.00 ..... | 4.25 ± 0.15 | 4.09 ± 0.20 | 3.86 ± 0.16 | 3.61 ± 0.13 |
| 291.34 ..... | 4.35 ± 0.14 | 3.84 ± 0.19 | 3.89 ± 0.15 | 3.72 ± 0.12 |
| 291.47 ..... | 4.39 ± 0.13 | 3.94 ± 0.17 | 3.84 ± 0.13 | 3.72 ± 0.11 |
| 291.74 ..... | 3.99 ± 0.15 | 3.58 ± 0.20 | 3.88 ± 0.16 | 3.86 ± 0.13 |
| 291.88 ..... | 4.10 ± 0.14 | 3.64 ± 0.19 | 3.78 ± 0.15 | 3.56 ± 0.12 |
| 292.01 ..... | 4.25 ± 0.17 | 4.04 ± 0.21 | 3.98 ± 0.17 | 3.64 ± 0.14 |
| 292.33 ..... | 4.37 ± 0.15 | 4.05 ± 0.20 | 3.82 ± 0.16 | 3.64 ± 0.13 |
| 292.47 ..... | 4.45 ± 0.14 | 3.92 ± 0.19 | 4.12 ± 0.15 | 3.63 ± 0.12 |
| 292.73 ..... | 4.42 ± 0.18 | 3.83 ± 0.23 | 3.83 ± 0.19 | 3.74 ± 0.15 |
| 292.85 ..... | 4.43 ± 0.15 | 4.09 ± 0.19 | 4.04 ± 0.16 | 3.84 ± 0.13 |
| 292.98 ..... | 4.37 ± 0.17 | 4.05 ± 0.22 | 4.01 ± 0.17 | 3.84 ± 0.14 |
| 293.33 ..... | 4.71 ± 0.17 | 4.45 ± 0.22 | 4.33 ± 0.17 | 3.78 ± 0.14 |
| 293.45 ..... | 4.52 ± 0.18 | 4.07 ± 0.24 | 4.14 ± 0.19 | 3.98 ± 0.15 |
| 293.59 ..... | 4.46 ± 0.14 | 4.15 ± 0.19 | 4.02 ± 0.15 | 3.95 ± 0.12 |
| 293.73 ..... | 4.69 ± 0.14 | 4.42 ± 0.19 | 4.00 ± 0.15 | 3.79 ± 0.12 |
| 293.85 ..... | 4.66 ± 0.19 | 4.27 ± 0.24 | 4.24 ± 0.20 | 3.97 ± 0.16 |
| 293.98 ..... | 4.74 ± 0.15 | 4.27 ± 0.19 | 4.10 ± 0.16 | 3.66 ± 0.13 |

NOTE.—Units are $10^{-14}$ ergs s$^{-1}$ cm$^{-2}$ Å$^{-1}$.

$N_{\rm data}$ in the TOMSIPS and NEWSIPS data is due to the fact that we have excluded from this (and forthcoming) analysis any points whose fluxes are more than 5 $\sigma$ away from both neighboring points. These outliers were rejected under the assumption that they are not due to intrinsic variability but rather are due to cosmic-ray hits or other unidentified defects in the original spectrum.

### 3.4. *Cross-Correlation Analysis*

In order to quantify the apparent time delays between the continuum and emission-line variations and to test for possible time delays between flux variations in different continuum bands, we performed a detailed cross-correlation analysis on both the TOMSIPS and NEWSIPS data.

We used two different algorithms to compute the cross-correlation functions (CCFs):

1. The interpolation CCF (ICCF) of Gaskell & Sparke (1986) and Gaskell & Peterson (1987) in the implementation of White & Peterson (1994).
2. The discrete CCF (DCF) of Edelson & Krolik (1988) in the implementation of White & Peterson (1994).

The CCF results from the TOMSIPS data are shown in Figure 5, whereas both NEWSIPS and TOMSIPS results are tabulated in Table 5. The NEWSIPS and TOMSIPS ICCFs and DCFs are identical to within the DCF error bars.

#### 3.4.1. *The Continuum Bands*

The most interesting cross-correlation results are the time delays observed between the different continuum bands. Adopting the continuum at 1315 Å as the driver, the other continuum wave bands lag behind with delays of $0^d.19$–$0^d.22$ (1485 Å), $0^d.32$–$0^d.38$ (1740 Å), and $0^d.22$–$0^d.35$ (1825 Å). The bounds given here are the differences in the CCF centroids determined from the measurements based on the TOMSIPS and NEWSIPS versions of the spectra. Taking the average of the two reduction methods, we have lags of $0^d.21$, $0^d.35$, and $0^d.28$, respectively. Throughout this paper, we will use the term "lag" as the time delay measured from the centroid of the CCF. We caution the reader that a "lag" does not imply a simple phase shift between two light curves.

This result was also tested by dividing the light curves into two approximately equal subsets and again performing cross correlations. This test yielded the same result for both halves of the light curves, thus demonstrating that the results obtained here are not attributable to some single feature in the light curves.

The centroids of the CCFs are calculated at 0.8 times the maximum correlation amplitude. If we calculate the centroids at 0.5 times the maximum, the continuum delays are slightly increased: for the TOMSIPS data, we find $0^d.23$, $0^d.35$, and $0^d.33$, respectively, for the three continuum bands, and for the NEWSIPS data, we find $0^d.28$, $0^d.37$, and $0^d.37$, respectively. However, we will discuss only the centroids at 0.8 times the maximum correlation amplitude as this value was also calculated in the many other AGN monitoring campaigns (see, e.g., Edelson et al. 1996) and allows for consistent comparison. The fact that the value of the centroid is a function of its definition emphasizes that the time relations between the different bands are not simple shifts.

The reason to use the CCF's centroid instead of its peak position as the definition of the lag between a continuum and an emission-line light curve is because the centroid of the CCF is directly related to the centroid of the transfer function of equation (1) (Koratkar & Gaskell 1991). The centroid lag is thus a measure of the "luminosity-weighted"

TABLE 3

EMISSION-LINE FLUXES (TOMSIPS)

| JD (−2,450,000) (1) | Lyα (2) | Lyα + N v (3) | N v (4) | Si iv (5) | C iv (6) | He ii (7) | C iii] (8) |
|---|---|---|---|---|---|---|---|
| 245.72 ..... | 220.1 ± 7.2 | 256.9 ± 10.7 | 36.7 ± 5.7 | 57.4 ± 8.7 | 293.4 ± 9.6 | 88.5 ± 11.9 | 64.3 ± 13.7 |
| 245.90 ..... | 231.3 ± 8.5 | 280.4 ± 12.7 | 49.1 ± 6.6 | 69.9 ± 10.2 | 297.7 ± 11.4 | 73.0 ± 14.2 | 54.0 ± 16.0 |
| 246.61 ..... | 232.1 ± 6.9 | 280.7 ± 10.3 | 48.6 ± 5.5 | 68.8 ± 8.1 | 306.0 ± 8.9 | 79.6 ± 11.4 | 64.1 ± 13.0 |
| 246.79 ..... | 229.7 ± 8.6 | 279.0 ± 12.8 | 49.3 ± 6.7 | 70.7 ± 10.2 | 309.6 ± 11.4 | 95.8 ± 14.2 | 53.1 ± 16.1 |
| 246.97 ..... | 219.3 ± 10.1 | 253.4 ± 15.1 | 34.1 ± 7.7 | 63.6 ± 12.1 | 279.4 ± 13.7 | 79.1 ± 16.8 | 66.0 ± 18.9 |
| 247.57 ..... | 220.2 ± 8.5 | 253.9 ± 12.4 | 33.7 ± 6.6 | 74.3 ± 10.5 | 297.7 ± 11.5 | 64.0 ± 14.1 | 56.9 ± 16.2 |
| 247.74 ..... | 238.1 ± 8.4 | 274.6 ± 12.5 | 36.4 ± 6.5 | 62.4 ± 10.0 | 282.9 ± 11.1 | 66.8 ± 13.9 | 53.3 ± 15.7 |
| 247.93 ..... | 232.8 ± 8.5 | 285.4 ± 12.7 | 52.5 ± 6.6 | 63.3 ± 10.1 | 304.8 ± 11.3 | 91.0 ± 14.1 | 69.0 ± 16.0 |
| 248.42 ..... | 228.6 ± 7.8 | 268.5 ± 11.5 | 39.9 ± 6.1 | 62.1 ± 9.4 | 277.8 ± 10.4 | 66.1 ± 12.8 | 53.4 ± 14.7 |
| 248.60 ..... | 243.0 ± 6.7 | 288.0 ± 9.9 | 45.0 ± 5.4 | 64.5 ± 8.2 | 298.8 ± 8.9 | 65.8 ± 11.0 | 59.8 ± 12.8 |
| 248.96 ..... | 229.1 ± 7.9 | 275.3 ± 11.6 | 46.2 ± 6.2 | 70.2 ± 9.5 | 283.0 ± 10.5 | 97.9 ± 13.0 | 59.6 ± 14.9 |
| 249.39 ..... | 228.2 ± 7.9 | 270.5 ± 11.6 | 42.3 ± 6.2 | 61.0 ± 9.5 | 289.0 ± 10.5 | 68.2 ± 13.0 | 69.4 ± 14.9 |
| 249.57 ..... | 229.4 ± 8.4 | 275.3 ± 12.4 | 45.9 ± 6.6 | 65.8 ± 10.3 | 301.6 ± 11.3 | 92.1 ± 13.9 | 72.8 ± 15.9 |
| 249.74 ..... | 217.5 ± 10.3 | 254.2 ± 15.4 | 36.7 ± 7.9 | 63.7 ± 12.3 | 288.0 ± 14.0 | 64.4 ± 17.2 | 52.1 ± 19.4 |
| 249.92 ..... | 226.3 ± 8.1 | 267.0 ± 12.0 | 40.7 ± 6.4 | 70.0 ± 9.8 | 310.1 ± 10.9 | 78.4 ± 13.4 | 71.5 ± 15.4 |
| 250.42 ..... | 245.2 ± 7.4 | 300.4 ± 10.9 | 55.3 ± 5.9 | 69.8 ± 8.9 | 300.5 ± 9.9 | 79.4 ± 12.2 | 65.3 ± 14.1 |
| 250.59 ..... | 232.7 ± 8.8 | 279.3 ± 13.0 | 46.5 ± 6.8 | 61.2 ± 10.5 | 298.2 ± 11.8 | 79.1 ± 14.5 | 62.5 ± 16.6 |
| 250.76 ..... | 229.5 ± 7.5 | 278.8 ± 11.0 | 49.3 ± 5.9 | 60.3 ± 9.0 | 296.6 ± 9.9 | 68.4 ± 12.3 | 60.3 ± 14.2 |
| 250.92 ..... | 228.8 ± 7.4 | 278.6 ± 10.9 | 49.9 ± 5.9 | 62.6 ± 9.0 | 310.1 ± 9.9 | 79.2 ± 12.2 | 76.5 ± 14.1 |
| 251.48 ..... | 245.4 ± 6.7 | 301.1 ± 9.8 | 55.7 ± 5.3 | 76.4 ± 8.1 | 306.8 ± 8.8 | 68.0 ± 11.0 | 57.9 ± 12.7 |
| 251.65 ..... | 233.4 ± 9.6 | 276.5 ± 14.3 | 43.1 ± 7.4 | 69.0 ± 11.5 | 300.7 ± 13.0 | 84.1 ± 15.9 | 66.6 ± 18.0 |
| 251.81 ..... | 229.2 ± 7.3 | 274.2 ± 10.8 | 45.0 ± 5.8 | 62.9 ± 8.8 | 283.0 ± 9.7 | 74.0 ± 12.0 | 51.4 ± 13.9 |
| 251.99 ..... | 226.7 ± 9.3 | 271.9 ± 14.0 | 45.2 ± 7.2 | 65.7 ± 11.1 | 303.4 ± 12.5 | 70.9 ± 15.5 | 65.8 ± 17.5 |
| 252.45 ..... | 222.8 ± 5.8 | 258.0 ± 8.4 | 35.2 ± 4.7 | 62.0 ± 7.0 | 296.5 ± 7.6 | 50.1 ± 9.5 | 51.9 ± 11.1 |
| 252.78 ..... | 212.2 ± 6.1 | 256.8 ± 8.9 | 44.6 ± 4.9 | 52.8 ± 7.5 | 284.5 ± 8.1 | 67.2 ± 10.0 | 67.4 ± 11.7 |
| 252.95 ..... | 220.7 ± 6.8 | 266.2 ± 10.0 | 45.5 ± 5.4 | 58.3 ± 8.2 | 297.8 ± 9.0 | 56.6 ± 11.2 | 68.2 ± 12.9 |
| 253.40 ..... | ... | ... | 29.8 ± 4.9 | 51.7 ± 7.6 | 254.7 ± 8.1 | 70.0 ± 10.0 | 84.7 ± 11.8 |
| 253.57 ..... | 199.7 ± 6.4 | 240.7 ± 9.4 | 40.9 ± 5.2 | 55.8 ± 7.8 | 276.2 ± 8.5 | 48.9 ± 10.6 | 71.0 ± 12.3 |
| 253.74 ..... | 198.8 ± 6.1 | 232.6 ± 8.9 | 33.8 ± 4.9 | 39.9 ± 7.4 | 279.4 ± 8.0 | 50.0 ± 9.9 | 95.8 ± 11.6 |
| 253.91 ..... | 201.1 ± 5.7 | 236.9 ± 8.3 | 35.8 ± 4.7 | 44.2 ± 7.2 | 281.1 ± 7.6 | 58.6 ± 9.5 | 73.6 ± 11.1 |
| 254.39 ..... | 216.0 ± 6.0 | 254.8 ± 8.8 | 38.8 ± 4.8 | 50.1 ± 7.2 | 254.4 ± 7.8 | 55.2 ± 9.9 | 68.3 ± 11.4 |
| 254.56 ..... | 198.2 ± 5.8 | 229.1 ± 8.4 | 30.9 ± 4.7 | 42.0 ± 7.1 | 266.2 ± 7.6 | 44.5 ± 9.5 | 51.6 ± 11.1 |
| 254.72 ..... | 198.9 ± 7.3 | 225.5 ± 10.8 | 26.6 ± 5.8 | 37.7 ± 8.9 | 267.5 ± 9.8 | 54.9 ± 12.1 | 71.2 ± 14.0 |
| 254.90 ..... | 193.4 ± 5.8 | 230.9 ± 8.6 | 37.6 ± 4.7 | 54.0 ± 7.1 | 269.4 ± 7.6 | 66.5 ± 9.6 | 74.0 ± 11.2 |
| 255.41 ..... | 206.7 ± 9.3 | 242.3 ± 14.1 | 35.6 ± 7.8 | 55.1 ± 11.2 | 248.7 ± 11.1 | 71.1 ± 14.8 | 66.5 ± 18.0 |
| 255.59 ..... | 201.8 ± 9.7 | 241.7 ± 14.4 | 39.9 ± 7.5 | 51.6 ± 11.8 | 283.2 ± 13.2 | 67.0 ± 16.1 | 68.4 ± 18.3 |
| 255.76 ..... | 195.6 ± 8.2 | 229.8 ± 12.1 | 34.2 ± 6.4 | 43.2 ± 9.8 | 269.9 ± 10.9 | 52.6 ± 13.5 | 64.8 ± 15.4 |
| 255.93 ..... | 207.5 ± 9.2 | 245.9 ± 13.6 | 38.3 ± 7.1 | 58.3 ± 11.0 | 281.8 ± 12.4 | 67.3 ± 15.2 | 67.0 ± 17.3 |
| 256.41 ..... | 207.8 ± 7.7 | 249.1 ± 11.4 | 41.3 ± 6.1 | 50.8 ± 9.3 | 271.7 ± 10.3 | 72.4 ± 12.7 | 67.1 ± 14.6 |
| 256.92 ..... | 209.6 ± 6.5 | 250.8 ± 9.5 | 41.2 ± 5.2 | 50.4 ± 7.8 | 265.3 ± 8.5 | 49.8 ± 10.7 | 49.3 ± 12.4 |
| 257.82 ..... | 190.6 ± 6.8 | 225.3 ± 9.9 | 34.7 ± 5.4 | 64.8 ± 8.3 | 253.4 ± 9.0 | 62.0 ± 11.2 | 64.4 ± 13.0 |
| 257.98 ..... | 196.0 ± 7.2 | 241.5 ± 10.7 | 45.5 ± 5.7 | 49.6 ± 8.6 | 273.4 ± 9.5 | 54.4 ± 11.9 | 63.1 ± 13.7 |
| 258.41 ..... | 194.3 ± 7.4 | 225.9 ± 10.9 | 31.6 ± 5.9 | 49.2 ± 8.9 | 248.7 ± 9.8 | 46.7 ± 12.2 | 48.6 ± 14.1 |
| 258.58 ..... | 200.9 ± 7.9 | 244.8 ± 11.7 | 43.9 ± 6.2 | 59.3 ± 9.5 | 263.1 ± 10.5 | 56.4 ± 13.0 | 51.5 ± 14.9 |
| 258.75 ..... | 192.0 ± 7.6 | 225.9 ± 11.2 | 33.9 ± 6.0 | 68.7 ± 9.1 | 264.5 ± 10.1 | 77.2 ± 12.5 | 68.8 ± 14.4 |
| 258.93 ..... | 194.3 ± 6.4 | 231.1 ± 9.4 | 36.8 ± 5.1 | 39.9 ± 7.7 | 261.0 ± 8.4 | 68.9 ± 10.5 | 55.2 ± 12.2 |
| 259.40 ..... | 207.5 ± 7.2 | 252.3 ± 10.5 | 44.8 ± 5.7 | 64.6 ± 8.7 | 258.7 ± 9.5 | 71.2 ± 11.8 | 59.7 ± 13.6 |
| 259.58 ..... | 204.8 ± 6.4 | 243.3 ± 9.3 | 38.5 ± 5.1 | 58.6 ± 7.8 | 263.5 ± 8.4 | 74.8 ± 10.5 | 60.2 ± 12.2 |
| 259.76 ..... | 198.7 ± 9.8 | 242.5 ± 14.6 | 43.8 ± 7.5 | 65.8 ± 11.7 | 255.6 ± 13.3 | 63.6 ± 16.3 | 53.7 ± 18.4 |
| 259.96 ..... | 187.4 ± 8.7 | 224.7 ± 12.8 | 37.3 ± 6.7 | 49.9 ± 10.5 | 257.8 ± 11.7 | 72.2 ± 14.4 | 64.8 ± 16.4 |
| 260.41 ..... | 213.0 ± 8.6 | 253.0 ± 12.7 | 39.9 ± 6.7 | 61.1 ± 10.3 | 269.7 ± 11.5 | 73.3 ± 14.2 | 58.7 ± 16.2 |
| 260.59 ..... | 209.1 ± 8.4 | 246.0 ± 12.5 | 36.9 ± 6.6 | 65.0 ± 10.1 | 286.4 ± 11.3 | 91.9 ± 13.9 | 86.3 ± 15.9 |
| 260.78 ..... | 192.2 ± 10.5 | 229.9 ± 15.6 | 37.7 ± 8.0 | 60.0 ± 12.5 | 261.4 ± 14.2 | 82.6 ± 17.4 | 67.2 ± 19.6 |
| 260.96 ..... | 202.2 ± 9.5 | 236.1 ± 14.1 | 33.8 ± 7.3 | 60.2 ± 11.3 | 269.8 ± 12.8 | 68.6 ± 15.7 | 80.3 ± 17.8 |
| 261.39 ..... | 206.2 ± 6.4 | 245.7 ± 9.4 | 39.4 ± 5.1 | 53.6 ± 7.7 | 261.8 ± 8.4 | 82.7 ± 10.5 | 57.7 ± 12.2 |
| 261.91 ..... | 203.4 ± 6.6 | 239.0 ± 9.6 | 35.6 ± 5.3 | 54.9 ± 8.0 | 255.1 ± 8.7 | 67.8 ± 10.8 | 56.1 ± 12.5 |
| 262.02 ..... | 194.6 ± 8.2 | 233.5 ± 12.2 | 39.0 ± 6.4 | 41.5 ± 10.0 | 261.7 ± 11.0 | 62.7 ± 13.6 | 52.3 ± 15.6 |
| 262.66 ..... | 192.8 ± 7.0 | 230.0 ± 10.4 | 37.3 ± 5.6 | 62.2 ± 8.5 | 255.1 ± 9.3 | 48.2 ± 11.6 | 55.7 ± 13.4 |
| 262.85 ..... | 200.0 ± 6.7 | 236.8 ± 9.9 | 36.8 ± 5.4 | 60.9 ± 8.2 | 271.0 ± 8.9 | 62.9 ± 11.1 | 62.8 ± 12.8 |
| 263.38 ..... | 194.7 ± 8.4 | 234.2 ± 12.4 | 39.5 ± 6.5 | 66.2 ± 10.2 | 264.9 ± 11.3 | 68.7 ± 13.9 | 55.5 ± 15.9 |
| 263.55 ..... | 195.9 ± 8.3 | 240.9 ± 12.2 | 45.0 ± 6.5 | 49.5 ± 9.9 | 272.8 ± 11.1 | 73.3 ± 13.6 | 54.8 ± 15.6 |
| 263.72 ..... | 202.4 ± 9.6 | 239.8 ± 14.3 | 37.4 ± 7.4 | 66.4 ± 11.7 | 271.0 ± 13.0 | 73.8 ± 16.0 | 56.7 ± 18.1 |
| 263.89 ..... | 195.9 ± 7.6 | 235.7 ± 11.2 | 39.8 ± 6.0 | 60.5 ± 9.2 | 259.8 ± 10.2 | 75.1 ± 12.6 | 51.8 ± 14.5 |
| 264.37 ..... | 191.4 ± 6.5 | 218.6 ± 9.5 | 27.2 ± 5.2 | 50.2 ± 7.9 | 261.3 ± 8.6 | 67.3 ± 10.7 | 53.9 ± 12.4 |
| 264.55 ..... | 190.2 ± 10.6 | 217.9 ± 15.8 | 27.7 ± 8.1 | 66.3 ± 12.8 | 272.0 ± 14.5 | 72.7 ± 17.6 | 65.3 ± 19.9 |
| 264.70 ..... | 195.9 ± 6.8 | 232.9 ± 10.0 | 36.9 ± 5.4 | 56.5 ± 8.3 | 267.8 ± 9.0 | 77.3 ± 11.2 | 43.0 ± 13.0 |
| 264.91 ..... | 186.8 ± 6.8 | 214.5 ± 10.0 | 27.7 ± 5.4 | 40.9 ± 8.3 | 252.5 ± 9.0 | 61.1 ± 11.2 | 46.8 ± 13.0 |
| 265.02 ..... | 198.2 ± 14.4 | 241.3 ± 21.6 | 43.1 ± 10.5 | 64.6 ± 17.2 | 286.0 ± 19.9 | 90.3 ± 24.1 | 66.4 ± 26.6 |
| 265.37 ..... | 194.9 ± 9.5 | 232.0 ± 14.2 | 37.1 ± 7.3 | 49.9 ± 11.4 | 260.6 ± 12.8 | 75.4 ± 15.8 | 48.4 ± 17.9 |
| 265.53 ..... | 202.0 ± 8.2 | 246.8 ± 12.0 | 44.8 ± 6.4 | 66.7 ± 9.9 | 281.1 ± 10.9 | 79.0 ± 13.5 | 48.8 ± 15.4 |
| 265.68 ..... | 203.2 ± 10.8 | 247.1 ± 16.1 | 43.9 ± 8.2 | 74.8 ± 12.8 | 277.3 ± 14.6 | 78.5 ± 17.9 | 59.7 ± 20.1 |
| 265.84 ..... | 207.6 ± 10.7 | 254.0 ± 16.1 | 46.5 ± 8.1 | 74.5 ± 12.6 | 270.1 ± 14.4 | 81.4 ± 17.9 | 50.7 ± 19.9 |

TABLE 3—*Continued*

| JD (−2,450,000) (1) | Lyα (2) | Lyα + N v (3) | N v (4) | Si iv (5) | C iv (6) | He ii (7) | C iii] (8) |
|---|---|---|---|---|---|---|---|
| 266.38 ..... | 202.8 ± 7.1 | 241.8 ± 10.4 | 39.1 ± 5.6 | 55.6 ± 8.5 | 270.6 ± 9.4 | 73.2 ± 11.6 | 53.6 ± 13.4 |
| 266.54 ..... | 212.4 ± 7.0 | 251.8 ± 10.3 | 39.4 ± 5.5 | 68.1 ± 8.4 | 292.7 ± 9.2 | 83.0 ± 11.5 | 65.2 ± 13.3 |
| 266.69 ..... | 206.5 ± 7.5 | 249.8 ± 11.0 | 43.3 ± 5.9 | 63.5 ± 9.0 | 285.1 ± 9.9 | 69.4 ± 12.3 | 56.7 ± 14.2 |
| 266.85 ..... | 227.8 ± 10.5 | 273.8 ± 15.8 | 46.0 ± 8.0 | 61.5 ± 12.1 | 287.0 ± 13.7 | 86.4 ± 17.3 | 65.1 ± 19.2 |
| 267.01 ..... | 212.8 ± 7.7 | 263.2 ± 11.4 | 50.4 ± 6.1 | 83.5 ± 9.3 | 267.2 ± 10.3 | 68.6 ± 12.7 | 49.2 ± 14.6 |
| 267.37 ..... | 213.2 ± 6.5 | 265.0 ± 9.5 | 51.8 ± 5.2 | 67.9 ± 7.9 | 315.4 ± 8.6 | 58.5 ± 10.7 | 61.9 ± 12.4 |
| 267.49 ..... | 205.3 ± 7.8 | 250.2 ± 11.5 | 44.9 ± 6.1 | 58.5 ± 9.5 | 263.3 ± 10.5 | 75.9 ± 12.9 | 51.5 ± 14.8 |
| 267.71 ..... | 204.9 ± 9.1 | 253.1 ± 13.6 | 48.2 ± 7.1 | 59.8 ± 10.9 | 278.8 ± 12.3 | 76.1 ± 15.1 | 60.9 ± 17.2 |
| 267.84 ..... | 206.1 ± 9.5 | 246.0 ± 14.2 | 39.9 ± 7.3 | 63.7 ± 11.4 | 305.1 ± 12.9 | 64.2 ± 15.8 | 59.3 ± 17.9 |
| 267.96 ..... | 211.9 ± 8.6 | 257.7 ± 12.7 | 45.8 ± 6.7 | 55.0 ± 10.5 | 281.2 ± 11.6 | 54.3 ± 14.3 | 51.0 ± 16.3 |
| 268.37 ..... | 199.2 ± 8.4 | 241.3 ± 12.3 | 42.1 ± 6.5 | 57.3 ± 10.2 | 261.3 ± 11.2 | 45.4 ± 13.8 | 47.7 ± 15.8 |
| 268.50 ..... | 207.8 ± 7.7 | 241.3 ± 11.3 | 33.5 ± 6.1 | 62.2 ± 9.4 | 261.2 ± 10.3 | 53.5 ± 12.7 | 62.4 ± 14.6 |
| 268.72 ..... | 203.0 ± 6.1 | 238.7 ± 8.9 | 35.7 ± 4.9 | 53.6 ± 7.6 | 271.9 ± 8.1 | 45.2 ± 10.1 | 55.0 ± 11.8 |
| 268.84 ..... | 209.3 ± 9.2 | 250.6 ± 13.7 | 41.4 ± 7.1 | 57.4 ± 11.2 | 280.4 ± 12.5 | 57.1 ± 15.3 | 51.3 ± 17.4 |
| 268.97 ..... | 189.1 ± 8.5 | 235.4 ± 12.5 | 46.3 ± 6.6 | 51.7 ± 10.3 | 269.9 ± 11.4 | 53.0 ± 14.0 | 56.3 ± 16.0 |
| 269.37 ..... | ... | ... | 32.1 ± 5.5 | 44.9 ± 8.7 | 248.0 ± 9.4 | 61.4 ± 11.5 | 60.6 ± 13.4 |
| 269.51 ..... | 205.4 ± 6.1 | 258.8 ± 8.9 | 53.4 ± 4.9 | 66.0 ± 7.6 | 277.2 ± 8.1 | 56.7 ± 10.1 | 58.5 ± 11.8 |
| 269.74 ..... | 216.8 ± 5.8 | 257.4 ± 8.6 | 40.6 ± 4.7 | 51.2 ± 6.9 | 294.2 ± 7.4 | 64.1 ± 9.5 | 64.0 ± 11.0 |
| 269.88 ..... | 204.0 ± 8.9 | 237.9 ± 13.2 | 33.9 ± 6.9 | 44.8 ± 10.7 | 279.4 ± 12.0 | 61.4 ± 14.8 | 82.3 ± 16.8 |
| 270.00 ..... | 188.1 ± 13.9 | 214.2 ± 21.0 | 26.1 ± 10.2 | 65.8 ± 16.5 | 293.8 ± 19.2 | 91.0 ± 23.3 | 60.1 ± 25.7 |
| 270.38 ..... | 197.0 ± 5.6 | 232.3 ± 8.1 | 35.3 ± 4.5 | 51.5 ± 6.8 | 281.5 ± 7.3 | 48.1 ± 9.1 | 52.6 ± 10.7 |
| 270.50 ..... | 197.1 ± 7.7 | 241.6 ± 11.4 | 44.5 ± 6.1 | 48.8 ± 9.3 | 268.9 ± 10.3 | 57.8 ± 12.7 | 56.9 ± 14.6 |
| 270.73 ..... | 198.7 ± 5.9 | 233.3 ± 8.7 | 34.6 ± 4.8 | 47.2 ± 7.2 | 272.4 ± 7.8 | 65.6 ± 9.7 | 60.0 ± 11.4 |
| 270.86 ..... | 193.2 ± 6.1 | 228.8 ± 8.9 | 35.6 ± 4.9 | 64.0 ± 7.4 | 265.0 ± 8.0 | 60.4 ± 10.0 | 59.2 ± 11.7 |
| 270.98 ..... | 198.8 ± 9.9 | 237.8 ± 14.8 | 39.0 ± 7.6 | 50.4 ± 11.8 | 258.0 ± 13.4 | 47.4 ± 16.5 | 44.4 ± 18.6 |
| 271.36 ..... | 198.2 ± 8.2 | 236.3 ± 12.1 | 38.0 ± 6.4 | 41.7 ± 9.8 | 283.0 ± 10.9 | 60.9 ± 13.5 | 54.9 ± 15.4 |
| 271.49 ..... | 186.3 ± 6.0 | 210.5 ± 8.8 | 24.2 ± 4.9 | 32.7 ± 7.3 | 268.7 ± 7.9 | 42.2 ± 9.8 | 58.1 ± 11.5 |
| 271.74 ..... | 192.9 ± 6.0 | 225.4 ± 8.8 | 32.5 ± 4.8 | 41.3 ± 7.3 | 263.6 ± 7.8 | 33.5 ± 9.8 | 56.3 ± 11.5 |
| 271.87 ..... | 193.2 ± 9.2 | 228.5 ± 13.7 | 35.3 ± 7.1 | 46.6 ± 11.1 | 267.2 ± 12.5 | 69.0 ± 15.3 | 70.8 ± 17.4 |
| 272.35 ..... | 194.0 ± 5.9 | 222.6 ± 8.7 | 28.6 ± 4.8 | 48.4 ± 7.1 | 256.4 ± 7.7 | 61.3 ± 9.7 | 63.1 ± 11.3 |
| 272.48 ..... | 183.5 ± 8.6 | 219.2 ± 12.7 | 35.7 ± 6.7 | 40.6 ± 10.3 | 253.2 ± 11.5 | 61.5 ± 14.2 | 61.3 ± 16.2 |
| 272.72 ..... | 190.9 ± 7.7 | 220.9 ± 11.4 | 30.0 ± 6.0 | 41.4 ± 9.2 | 245.4 ± 10.2 | 53.5 ± 12.7 | 65.9 ± 14.5 |
| 272.85 ..... | 187.7 ± 7.0 | 221.9 ± 10.3 | 34.2 ± 5.5 | 42.2 ± 8.3 | 240.9 ± 9.1 | 58.1 ± 11.5 | 65.1 ± 13.2 |
| 272.97 ..... | 179.7 ± 6.7 | 207.0 ± 9.8 | 27.3 ± 5.3 | 28.6 ± 8.1 | 236.1 ± 8.8 | 32.5 ± 11.0 | 62.9 ± 12.7 |
| 273.36 ..... | 177.7 ± 5.3 | 208.1 ± 7.7 | 30.3 ± 4.4 | 39.7 ± 6.5 | 244.5 ± 6.9 | 55.7 ± 8.7 | 61.4 ± 10.2 |
| 273.49 ..... | 172.5 ± 7.5 | 198.2 ± 11.1 | 25.7 ± 5.9 | 39.2 ± 9.2 | 251.1 ± 10.1 | 56.4 ± 12.4 | 78.6 ± 14.3 |
| 273.73 ..... | 170.3 ± 6.3 | 196.7 ± 9.3 | 26.3 ± 5.1 | 43.9 ± 7.7 | 238.6 ± 8.3 | 47.8 ± 10.4 | 60.8 ± 12.1 |
| 273.87 ..... | 197.5 ± 6.6 | 236.7 ± 9.8 | 39.3 ± 5.3 | 37.7 ± 8.0 | 237.5 ± 8.8 | 50.3 ± 10.9 | 54.3 ± 12.7 |
| 274.02 ..... | 176.7 ± 9.3 | 212.6 ± 13.8 | 36.0 ± 7.2 | 37.5 ± 11.1 | 251.8 ± 12.5 | 48.8 ± 15.4 | 52.6 ± 17.5 |
| 274.36 ..... | 165.1 ± 5.1 | 193.8 ± 7.4 | 28.7 ± 4.2 | 31.8 ± 6.2 | 242.3 ± 6.6 | 59.2 ± 8.4 | 55.4 ± 9.8 |
| 274.49 ..... | 171.5 ± 9.3 | 204.0 ± 13.8 | 32.5 ± 7.2 | 46.9 ± 11.3 | 245.0 ± 12.6 | 51.9 ± 15.4 | 59.3 ± 17.5 |
| 274.76 ..... | 182.6 ± 6.0 | 214.1 ± 8.8 | 31.5 ± 4.8 | 37.6 ± 7.1 | 249.4 ± 7.7 | 50.0 ± 9.8 | 57.7 ± 11.3 |
| 274.89 ..... | 177.3 ± 7.1 | 204.6 ± 10.4 | 27.3 ± 5.6 | 37.4 ± 8.6 | 266.0 ± 9.4 | 57.5 ± 11.7 | 56.2 ± 13.5 |
| 275.01 ..... | 180.2 ± 9.3 | 208.1 ± 13.9 | 27.9 ± 7.2 | 31.8 ± 11.2 | 222.5 ± 12.6 | 44.5 ± 15.5 | 51.2 ± 17.6 |
| 275.35 ..... | 171.9 ± 6.0 | 196.5 ± 8.8 | 24.7 ± 4.9 | 40.1 ± 7.4 | 245.4 ± 8.0 | 50.1 ± 9.9 | 53.2 ± 11.6 |
| 275.48 ..... | 178.8 ± 6.3 | 213.8 ± 9.2 | 35.0 ± 5.1 | 34.8 ± 7.7 | 254.4 ± 8.3 | 67.8 ± 10.3 | 61.7 ± 12.0 |
| 275.74 ..... | 172.3 ± 6.5 | 203.2 ± 9.5 | 30.9 ± 5.2 | 41.6 ± 7.8 | 253.0 ± 8.5 | 64.5 ± 10.7 | 52.9 ± 12.4 |
| 275.88 ..... | 191.5 ± 7.5 | 225.7 ± 11.0 | 34.2 ± 5.9 | 44.7 ± 9.0 | 262.5 ± 10.0 | 70.4 ± 12.3 | 58.9 ± 14.2 |
| 276.00 ..... | 173.9 ± 12.2 | 203.8 ± 18.3 | 29.8 ± 9.1 | 42.8 ± 14.5 | 254.9 ± 16.7 | 102.5 ± 20.4 | 67.6 ± 22.7 |
| 276.34 ..... | 200.1 ± 7.6 | 241.5 ± 11.2 | 41.4 ± 5.9 | 45.9 ± 9.0 | 262.6 ± 10.0 | 54.9 ± 12.5 | 48.8 ± 14.3 |
| 276.48 ..... | 191.3 ± 6.6 | 236.5 ± 9.7 | 45.2 ± 5.3 | 51.8 ± 7.9 | 256.5 ± 8.6 | 79.3 ± 10.8 | 50.8 ± 12.5 |
| 276.75 ..... | 192.8 ± 8.5 | 228.9 ± 12.6 | 36.0 ± 6.6 | 42.2 ± 10.2 | 265.1 ± 11.4 | 79.1 ± 14.0 | 64.8 ± 16.0 |
| 276.88 ..... | 182.2 ± 7.6 | 214.4 ± 11.2 | 32.2 ± 6.0 | 33.8 ± 9.1 | 289.5 ± 10.0 | 72.7 ± 12.5 | 52.1 ± 14.3 |
| 277.01 ..... | 185.7 ± 8.6 | 224.1 ± 12.8 | 38.3 ± 6.7 | 48.1 ± 10.3 | 285.9 ± 11.5 | 76.6 ± 14.2 | 82.9 ± 16.2 |
| 277.35 ..... | 201.6 ± 7.5 | 231.9 ± 11.1 | 30.4 ± 5.9 | 40.9 ± 9.0 | 280.6 ± 10.0 | 68.2 ± 12.4 | 54.4 ± 14.2 |
| 277.49 ..... | 198.1 ± 9.7 | 237.3 ± 14.4 | 39.3 ± 7.4 | 52.5 ± 11.6 | 267.0 ± 13.1 | 59.4 ± 16.0 | 61.1 ± 18.2 |
| 277.78 ..... | 195.8 ± 6.8 | 243.2 ± 9.9 | 47.5 ± 5.4 | 56.8 ± 8.2 | 275.7 ± 8.9 | 72.9 ± 11.1 | 56.5 ± 12.9 |
| 277.90 ..... | 200.9 ± 10.2 | 245.0 ± 15.3 | 44.0 ± 7.8 | 42.0 ± 12.2 | 283.5 ± 13.9 | 61.7 ± 17.0 | 43.6 ± 19.1 |
| 278.03 ..... | 182.7 ± 11.3 | 218.0 ± 17.0 | 35.2 ± 8.5 | 51.7 ± 13.5 | 268.1 ± 15.5 | 70.5 ± 18.9 | 64.1 ± 21.1 |
| 278.34 ..... | 195.9 ± 8.0 | 237.9 ± 11.9 | 42.0 ± 6.3 | 58.2 ± 9.6 | 274.4 ± 10.7 | 86.5 ± 13.2 | 58.1 ± 15.2 |
| 278.47 ..... | 178.8 ± 7.4 | 215.0 ± 10.9 | 36.2 ± 5.9 | 45.8 ± 8.9 | 271.5 ± 9.9 | 70.7 ± 12.2 | 68.9 ± 14.1 |
| 278.76 ..... | 195.0 ± 7.2 | 239.3 ± 10.7 | 44.3 ± 5.7 | 48.5 ± 8.7 | 263.3 ± 9.6 | 35.3 ± 11.9 | 51.4 ± 13.7 |
| 279.33 ..... | 190.3 ± 8.2 | 221.0 ± 12.1 | 30.7 ± 6.4 | 40.4 ± 9.7 | 270.5 ± 10.8 | 73.1 ± 13.5 | 57.3 ± 15.4 |
| 279.46 ..... | 190.8 ± 6.1 | 231.3 ± 8.9 | 40.5 ± 4.9 | 49.8 ± 7.4 | 284.0 ± 8.0 | 70.9 ± 10.0 | 56.2 ± 11.6 |
| 279.75 ..... | 199.9 ± 7.2 | 244.9 ± 10.6 | 45.0 ± 5.7 | 52.8 ± 8.6 | 275.6 ± 9.4 | 56.5 ± 11.8 | 41.4 ± 13.6 |
| 279.89 ..... | 202.2 ± 6.8 | 245.2 ± 10.0 | 43.0 ± 5.4 | 46.5 ± 8.0 | 263.1 ± 8.7 | 42.1 ± 11.1 | 45.0 ± 12.7 |
| 280.02 ..... | ... | 281.0 ± 11.8 | 43.7 ± 6.2 | 64.5 ± 9.5 | 280.9 ± 10.5 | 83.6 ± 13.2 | 57.8 ± 15.0 |
| 280.34 ..... | 203.5 ± 6.3 | 239.0 ± 9.3 | 35.6 ± 5.0 | 41.1 ± 7.3 | 268.7 ± 8.0 | 57.8 ± 10.3 | 64.2 ± 11.8 |
| 280.47 ..... | 195.1 ± 7.1 | 230.7 ± 10.5 | 35.6 ± 5.6 | 40.3 ± 8.5 | 270.4 ± 9.4 | 60.8 ± 11.8 | 72.0 ± 13.5 |
| 280.74 ..... | 193.4 ± 7.7 | 230.9 ± 11.4 | 37.5 ± 6.1 | 29.4 ± 9.3 | 267.7 ± 10.3 | 61.6 ± 12.7 | 45.2 ± 14.6 |
| 280.88 ..... | 173.7 ± 7.4 | 205.1 ± 10.9 | 31.4 ± 5.8 | 36.1 ± 8.9 | 278.0 ± 9.8 | 76.6 ± 12.2 | 72.8 ± 14.0 |
| 281.01 ..... | 178.9 ± 8.6 | 214.6 ± 12.8 | 35.7 ± 6.7 | 40.6 ± 10.4 | 252.1 ± 11.6 | 57.7 ± 14.3 | 102.4 ± 16.3 |
| 281.34 ..... | 183.2 ± 6.3 | 215.6 ± 9.2 | 32.4 ± 5.0 | 47.4 ± 7.6 | 251.8 ± 8.2 | 55.4 ± 10.3 | 55.6 ± 12.0 |

TABLE 3—*Continued*

| JD (−2,450,000) (1) | Lyα (2) | Lyα + N v (3) | N v (4) | Si iv (5) | C iv (6) | He ii (7) | C iii] (8) |
|---|---|---|---|---|---|---|---|
| 281.47 ..... | 176.2 ± 5.8 | 207.9 ± 8.5 | 31.7 ± 4.7 | 37.2 ± 7.0 | ... | 48.6 ± 9.5 | 60.2 ± 11.1 |
| 281.75 ..... | 191.3 ± 5.8 | 225.8 ± 8.5 | 34.4 ± 4.7 | 46.5 ± 6.9 | 247.1 ± 7.5 | 45.6 ± 9.5 | 55.8 ± 11.1 |
| 282.35 ..... | 184.2 ± 7.5 | 221.6 ± 11.0 | 37.4 ± 5.9 | 40.9 ± 9.0 | 249.3 ± 9.9 | 41.9 ± 12.3 | 28.1 ± 14.2 |
| 282.49 ..... | 176.7 ± 7.6 | 214.3 ± 11.2 | 37.6 ± 6.0 | 30.4 ± 9.2 | 247.9 ± 10.1 | 40.4 ± 12.5 | 9.5 ± 14.4 |
| 282.77 ..... | 185.9 ± 6.9 | 221.8 ± 10.1 | 35.9 ± 5.4 | 47.8 ± 8.2 | 257.0 ± 9.0 | 47.6 ± 11.3 | 50.9 ± 13.0 |
| 282.89 ..... | ... | ... | 14.7 ± 5.2 | 20.1 ± 7.9 | 247.5 ± 8.6 | 39.4 ± 10.7 | 51.4 ± 12.4 |
| 283.02 ..... | 188.4 ± 8.3 | 211.4 ± 12.2 | 23.0 ± 6.5 | 45.0 ± 9.9 | 263.7 ± 11.1 | 52.3 ± 13.7 | 53.9 ± 15.6 |
| 283.34 ..... | 179.2 ± 6.3 | 206.6 ± 9.2 | 27.4 ± 5.0 | 43.3 ± 7.6 | 250.5 ± 8.2 | 57.9 ± 10.3 | 46.9 ± 12.0 |
| 283.47 ..... | 179.9 ± 7.8 | 213.4 ± 11.6 | 33.5 ± 6.1 | 46.0 ± 9.4 | 257.7 ± 10.4 | 82.9 ± 12.9 | 50.9 ± 14.8 |
| 283.74 ..... | 169.4 ± 7.8 | 195.9 ± 11.5 | 26.5 ± 6.1 | 50.4 ± 9.4 | 262.2 ± 10.4 | 56.3 ± 12.9 | 56.8 ± 14.8 |
| 283.88 ..... | 190.8 ± 6.4 | 222.7 ± 9.4 | 31.9 ± 5.2 | 32.2 ± 7.8 | 258.1 ± 8.4 | 62.5 ± 10.6 | 57.4 ± 12.3 |
| 284.00 ..... | 175.0 ± 6.8 | 200.6 ± 10.1 | 25.6 ± 5.4 | 42.1 ± 8.2 | 255.1 ± 9.0 | 96.0 ± 11.2 | 66.2 ± 13.0 |
| 284.35 ..... | 188.2 ± 7.7 | 216.6 ± 11.5 | 28.4 ± 6.1 | 42.6 ± 9.2 | 259.8 ± 10.2 | 37.7 ± 12.8 | 47.6 ± 14.6 |
| 284.47 ..... | 178.4 ± 6.6 | 220.9 ± 9.6 | 42.5 ± 5.2 | 55.6 ± 7.9 | 264.8 ± 8.6 | 51.9 ± 10.8 | 47.5 ± 12.5 |
| 284.74 ..... | 163.9 ± 7.5 | 191.5 ± 11.1 | 27.6 ± 5.9 | 28.1 ± 9.0 | 258.4 ± 10.0 | 52.3 ± 12.3 | 55.5 ± 14.2 |
| 284.89 ..... | 168.5 ± 6.2 | 194.9 ± 9.1 | 26.4 ± 5.0 | 38.3 ± 7.5 | 261.8 ± 8.1 | 76.0 ± 10.2 | 69.7 ± 11.9 |
| 285.01 ..... | 174.4 ± 9.6 | 194.7 ± 14.3 | 20.3 ± 7.4 | 41.5 ± 11.5 | 238.1 ± 12.9 | 28.4 ± 15.9 | 38.0 ± 18.0 |
| 285.49 ..... | 185.3 ± 11.6 | 231.1 ± 17.4 | 45.8 ± 8.7 | 41.2 ± 13.8 | 270.0 ± 15.9 | 58.6 ± 19.4 | 55.0 ± 21.6 |
| 285.76 ..... | 166.0 ± 5.7 | 196.5 ± 8.2 | 30.5 ± 4.6 | 36.5 ± 6.9 | 257.2 ± 7.4 | 50.9 ± 9.3 | 56.4 ± 10.9 |
| 285.88 ..... | 168.8 ± 7.4 | 202.6 ± 10.9 | 33.8 ± 5.9 | 41.9 ± 9.1 | 253.1 ± 9.9 | 53.8 ± 12.2 | 53.2 ± 14.1 |
| 286.01 ..... | 155.3 ± 8.8 | 178.6 ± 13.0 | 23.3 ± 6.8 | 32.1 ± 10.7 | 240.6 ± 11.9 | 43.6 ± 14.6 | 62.8 ± 16.6 |
| 286.34 ..... | 180.4 ± 8.3 | 218.1 ± 12.4 | 37.7 ± 6.5 | 44.1 ± 10.0 | 240.4 ± 11.2 | 55.6 ± 13.8 | 51.0 ± 15.8 |
| 286.47 ..... | 164.9 ± 5.3 | ... | 20.4 ± 4.4 | 22.7 ± 6.5 | 242.5 ± 7.0 | 39.6 ± 8.7 | 53.7 ± 10.3 |
| 286.74 ..... | 185.2 ± 8.7 | 218.8 ± 12.9 | 33.7 ± 6.7 | 42.5 ± 10.4 | 238.3 ± 11.7 | 15.5 ± 14.4 | ... |
| 286.86 ..... | 174.0 ± 6.0 | 205.4 ± 8.8 | 31.4 ± 4.9 | 42.9 ± 7.4 | 233.7 ± 7.9 | 39.8 ± 9.9 | 58.7 ± 11.6 |
| 286.99 ..... | 165.3 ± 6.3 | 191.1 ± 9.2 | 25.8 ± 5.0 | 19.5 ± 7.6 | 227.9 ± 8.2 | 38.8 ± 10.3 | 62.0 ± 12.0 |
| 287.33 ..... | 170.3 ± 5.3 | 191.2 ± 7.7 | 20.9 ± 4.3 | 30.7 ± 6.5 | 237.3 ± 6.9 | 35.6 ± 8.7 | 53.8 ± 10.2 |
| 287.46 ..... | 164.9 ± 5.2 | 186.1 ± 7.6 | 21.2 ± 4.3 | 20.0 ± 6.3 | 230.1 ± 6.7 | 33.7 ± 8.5 | 59.3 ± 10.0 |
| 287.74 ..... | 162.4 ± 7.3 | 186.2 ± 10.9 | 23.8 ± 5.8 | 35.9 ± 8.6 | 222.9 ± 9.4 | 49.6 ± 12.0 | 57.2 ± 13.7 |
| 287.88 ..... | 164.8 ± 8.3 | 189.9 ± 12.3 | 25.1 ± 6.5 | 44.5 ± 10.0 | 238.0 ± 11.1 | 37.3 ± 13.8 | 40.5 ± 15.7 |
| 288.00 ..... | 148.1 ± 6.8 | 166.6 ± 10.0 | 18.5 ± 5.4 | 25.9 ± 8.3 | 211.8 ± 9.0 | 37.8 ± 11.2 | 67.3 ± 13.0 |
| 288.34 ..... | 156.3 ± 7.5 | 178.5 ± 11.0 | 22.2 ± 5.9 | 30.8 ± 9.0 | 217.5 ± 9.9 | 47.3 ± 12.3 | 60.6 ± 14.2 |
| 288.46 ..... | 152.3 ± 7.1 | 165.7 ± 10.5 | 13.4 ± 5.7 | 14.2 ± 8.6 | 217.2 ± 9.5 | 27.3 ± 11.8 | 47.3 ± 13.6 |
| 288.74 ..... | 156.8 ± 6.0 | 182.0 ± 8.8 | 25.2 ± 4.9 | 42.2 ± 7.3 | 224.1 ± 7.9 | 35.4 ± 9.9 | 54.9 ± 11.6 |
| 288.87 ..... | 150.4 ± 6.3 | 167.9 ± 9.3 | 17.4 ± 5.1 | 20.0 ± 7.7 | 212.4 ± 8.4 | 68.3 ± 10.4 | 64.4 ± 12.1 |
| 288.99 ..... | 148.6 ± 7.7 | 174.7 ± 11.2 | 26.0 ± 6.0 | 23.5 ± 9.3 | 215.5 ± 10.2 | 37.6 ± 12.6 | 60.7 ± 14.5 |
| 289.34 ..... | 150.6 ± 5.4 | 169.8 ± 7.8 | 19.3 ± 4.4 | 24.3 ± 6.6 | 215.5 ± 7.0 | 45.6 ± 8.8 | 41.3 ± 10.3 |
| 289.46 ..... | 155.4 ± 5.7 | 174.0 ± 8.3 | 18.6 ± 4.6 | 30.6 ± 6.9 | 211.8 ± 7.4 | 38.9 ± 9.3 | 51.9 ± 10.9 |
| 289.73 ..... | 150.0 ± 6.9 | 175.3 ± 10.2 | 25.3 ± 5.5 | 35.3 ± 8.4 | 215.6 ± 9.2 | 37.0 ± 11.4 | 35.1 ± 13.2 |
| 289.87 ..... | 146.0 ± 7.4 | 165.8 ± 10.9 | 19.8 ± 5.8 | 24.1 ± 8.8 | 206.4 ± 9.7 | 49.2 ± 12.2 | 41.4 ± 13.9 |
| 290.00 ..... | 148.0 ± 6.5 | 178.0 ± 9.6 | 30.0 ± 5.2 | 32.6 ± 7.9 | 212.2 ± 8.6 | 58.9 ± 10.8 | 54.0 ± 12.5 |
| 290.33 ..... | 159.0 ± 8.0 | 188.8 ± 12.1 | 29.8 ± 6.2 | 32.4 ± 9.1 | 198.8 ± 10.1 | 54.2 ± 13.2 | 41.4 ± 14.7 |
| 290.46 ..... | 144.5 ± 6.0 | 170.9 ± 8.9 | 26.4 ± 4.8 | 32.7 ± 7.0 | 197.9 ± 7.6 | 35.9 ± 9.9 | 35.7 ± 11.3 |
| 290.73 ..... | 153.7 ± 8.4 | 170.4 ± 12.3 | 16.7 ± 6.5 | 39.6 ± 10.1 | 234.3 ± 11.2 | 62.4 ± 13.8 | 48.8 ± 15.8 |
| 290.87 ..... | 164.5 ± 9.9 | 193.5 ± 14.7 | 29.0 ± 7.6 | 33.0 ± 12.0 | 237.0 ± 13.5 | 64.7 ± 16.5 | 47.0 ± 18.6 |
| 291.00 ..... | 155.7 ± 7.5 | 181.9 ± 11.1 | 26.3 ± 5.9 | 37.8 ± 9.0 | 229.2 ± 10.0 | 61.7 ± 12.4 | 52.2 ± 14.2 |
| 291.34 ..... | 174.1 ± 6.6 | 204.2 ± 9.7 | 30.0 ± 5.3 | 40.1 ± 8.0 | 236.7 ± 8.7 | 37.5 ± 10.8 | 44.2 ± 12.6 |
| 291.47 ..... | 160.1 ± 5.8 | 179.2 ± 8.5 | 19.1 ± 4.7 | 41.7 ± 7.0 | 225.4 ± 7.6 | 53.2 ± 9.5 | 50.5 ± 11.1 |
| 291.74 ..... | 176.5 ± 7.9 | 210.3 ± 11.6 | 33.7 ± 6.2 | 42.8 ± 9.5 | 252.8 ± 10.5 | 65.2 ± 13.0 | 33.5 ± 14.9 |
| 291.88 ..... | 159.8 ± 6.5 | 190.2 ± 9.5 | 30.5 ± 5.2 | 47.1 ± 7.9 | 244.8 ± 8.5 | 93.2 ± 10.6 | 57.2 ± 12.3 |
| 292.01 ..... | 150.5 ± 8.6 | 175.1 ± 12.7 | 24.6 ± 6.7 | 36.6 ± 10.3 | 251.9 ± 11.5 | 58.5 ± 14.2 | 47.7 ± 16.2 |
| 292.33 ..... | 160.8 ± 7.6 | 189.5 ± 11.3 | 28.7 ± 6.0 | 40.8 ± 9.1 | 218.9 ± 10.0 | 66.8 ± 12.6 | 50.8 ± 14.3 |
| 292.47 ..... | 172.3 ± 7.0 | 203.3 ± 10.4 | 31.0 ± 5.6 | 36.0 ± 8.4 | 228.0 ± 9.2 | 60.3 ± 11.6 | 54.8 ± 13.3 |
| 292.73 ..... | 158.0 ± 9.8 | 181.5 ± 14.6 | 23.5 ± 7.5 | 37.8 ± 11.7 | 239.3 ± 13.2 | 71.7 ± 16.2 | 53.5 ± 18.3 |
| 292.85 ..... | 168.5 ± 7.0 | 200.3 ± 10.3 | 31.9 ± 5.6 | 38.7 ± 8.5 | 245.1 ± 9.3 | 58.0 ± 11.6 | 53.5 ± 13.4 |
| 292.98 ..... | 161.0 ± 9.1 | 192.6 ± 13.5 | 31.6 ± 7.0 | 45.7 ± 11.1 | 239.0 ± 12.3 | 48.3 ± 15.1 | 52.4 ± 17.2 |
| 293.33 ..... | 163.9 ± 8.8 | 188.8 ± 13.2 | 24.9 ± 6.8 | 40.6 ± 10.5 | 239.1 ± 11.8 | 77.8 ± 14.7 | 59.3 ± 16.6 |
| 293.45 ..... | 177.4 ± 10.3 | 201.4 ± 15.5 | 24.0 ± 7.8 | 42.6 ± 12.2 | 240.5 ± 13.9 | 58.2 ± 17.3 | 36.7 ± 19.3 |
| 293.59 ..... | 173.1 ± 6.8 | 199.8 ± 10.0 | 26.7 ± 5.4 | 49.2 ± 8.2 | 235.7 ± 8.9 | 51.7 ± 11.2 | 44.5 ± 12.9 |
| 293.73 ..... | 140.4 ± 6.5 | 160.3 ± 9.5 | 19.8 ± 5.2 | 44.6 ± 7.8 | 220.1 ± 8.5 | 65.5 ± 10.6 | 48.1 ± 12.3 |
| 293.85 ..... | 151.9 ± 10.8 | 177.4 ± 16.1 | 25.4 ± 8.2 | 36.9 ± 12.8 | 229.4 ± 14.6 | 50.1 ± 17.9 | 38.1 ± 20.1 |
| 293.98 ..... | 141.9 ± 6.8 | 160.3 ± 10.0 | 18.4 ± 5.4 | 55.6 ± 8.3 | 232.5 ± 9.0 | 63.3 ± 11.2 | 58.5 ± 13.0 |

NOTE.—Units are $10^{-14}$ ergs cm$^{-2}$ s$^{-1}$.

radius of the BLR. The interpretation of peak lag of the CCF, on the other hand, depends on the geometry of the reprocessing region and is often biased toward the inner regions of the reprocessing region. Furthermore, the peak lag also depends on sampling and continuum-variability characteristics.

The level of significance that can be ascribed to the detected time delays between the variations in the different UV continuum bands depends on accurate determination of the uncertainties in the time delays. Unfortunately, no completely plausible and robust method has yet emerged to assess the errors in cross-correlation lags derived from limited, irregularly sampled, noisy data. Monte Carlo simulations are often employed to assess these uncertainties, but

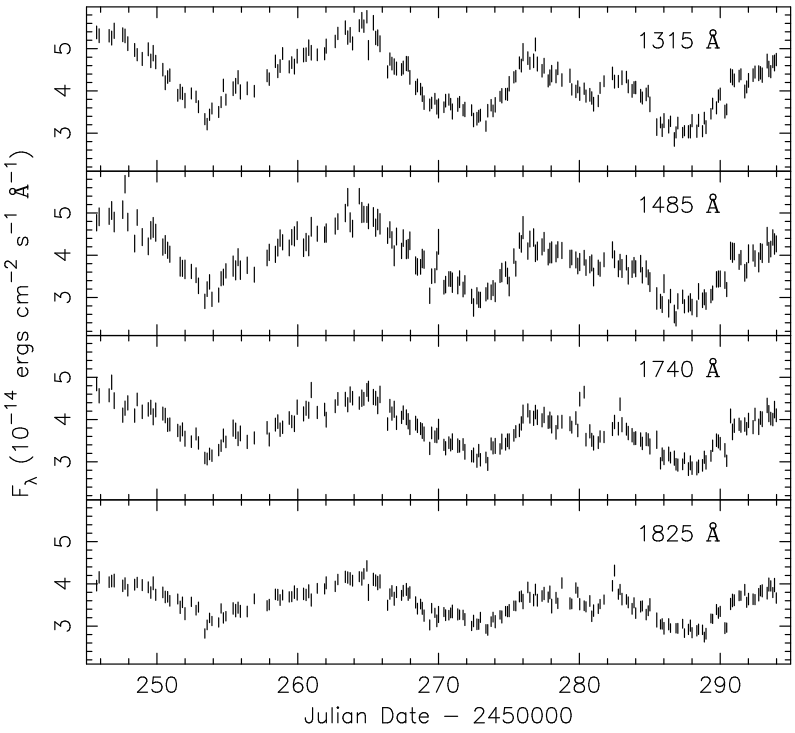


FIG. 4*a*

FIG. 4.—Continuum (*a*) and emission-line (*b*) flux light curves of the NGC 7469 TOMSIPS-reduced data and the 1 $\sigma$ errors

of course these are only as reliable as the input model that is used. Here, we employ a simple model and Monte Carlo simulations in an effort to obtain a quantitative estimate of the accuracy of the lag determinations. The fluxes of both the driving and responding light curves were reshuffled randomly using Gaussian deviates based on the quoted uncertainties for each data point. This was done 100 times. For each realization, we then computed the CCF and determined the lag. We thus obtained 100 lag estimates for each pair of light curves. The standard deviation of the distribution of lags around the mean was slightly less than $0\overset{d}{.}07$ for each pair of light curves. We therefore adopt $0\overset{d}{.}07$ as an estimate of the accuracy with which we can measure the lag between the different UV continuum wavebands. This is about 3 times smaller than the average sampling interval of about $0\overset{d}{.}2$ (the total integration time for each observation is about $0\overset{d}{.}1$, and the remaining gaps in coverage are due to overheads associated with satellite control and camera preparation). It is possible to measure lags smaller than the sampling interval because the variations on the shortest timescales sampled are apparently very smooth. This assumption will be justified elsewhere (Welsh et al. 1997), based on very high time-resolution, high signal-to-noise ratio spectra that were obtained with *HST* in order to search for rapid continuum variability during this monitoring campaign.

### 3.4.2. *The Emission Lines*

As expected from inspection of the light curves and the rms spectrum, the correlation between the continuum and

TABLE 4

VARIABILITY PARAMETERS

| | $N_{data}$ | | $\bar{F}$[a] | | $\sigma_F$[a] | | $F_{var}$ | | $R_{max}$ | |
|---|---|---|---|---|---|---|---|---|---|---|
| FEATURE (1) | N (2) | T (3) | N (4) | T (5) | N (6) | T (7) | N (8) | T (9) | N (10) | T (11) |
| $F_\lambda$(1315 Å)..... | 207 | 206 | 4.19 | 4.20 | 0.68 | 0.65 | 0.15 | 0.15 | 2.01 | 2.02 |
| $F_\lambda$(1485 Å)..... | 205 | 206 | 4.00 | 3.87 | 0.62 | 0.63 | 0.14 | 0.15 | 2.18 | 2.28 |
| $F_\lambda$(1740 Å)..... | 205 | 207 | 3.85 | 3.77 | 0.51 | 0.47 | 0.13 | 0.12 | 1.84 | 1.73 |
| $F_\lambda$(1825 Å)..... | 200 | 206 | 3.77 | 3.54 | 0.39 | 0.36 | 0.10 | 0.10 | 1.70 | 1.61 |
| Lyα..... | 206 | 203 | 227.2 | 190.8 | 25.8 | 22.9 | 0.10 | 0.11 | 1.70 | 1.75 |
| Lyα + N v..... | 206 | 203 | 267.9 | 226.3 | 34.2 | 30.3 | 0.10 | 0.12 | 1.90 | 1.88 |
| N v..... | 207 | 207 | 40.7 | 35.0 | 9.9 | 8.6 | 0.14 | 0.17 | 4.58 | 4.15 |
| Si IV..... | 205 | 207 | 55.4 | 48.6 | 11.9 | 13.1 | 0.17 | 0.19 | 3.69 | 5.86 |
| C IV..... | 204 | 206 | 253.6 | 261.5 | 26.3 | 23.9 | 0.09 | 0.08 | 1.70 | 1.59 |
| He II..... | 203 | 207 | 44.1 | 61.7 | 18.0 | 15.4 | ... | (0.14) | (248.1) | (6.59) |
| C III]..... | 199 | 206 | 65.9 | 57.6 | 15.2 | 10.9 | ... | ... | (7.90) | (10.81) |

[a] Units are $10^{-14}$ ergs cm$^{-2}$ s$^{-1}$ Å$^{-1}$ for continuum fluxes and $10^{-14}$ ergs cm$^{-2}$ s$^{-1}$ for line fluxes.

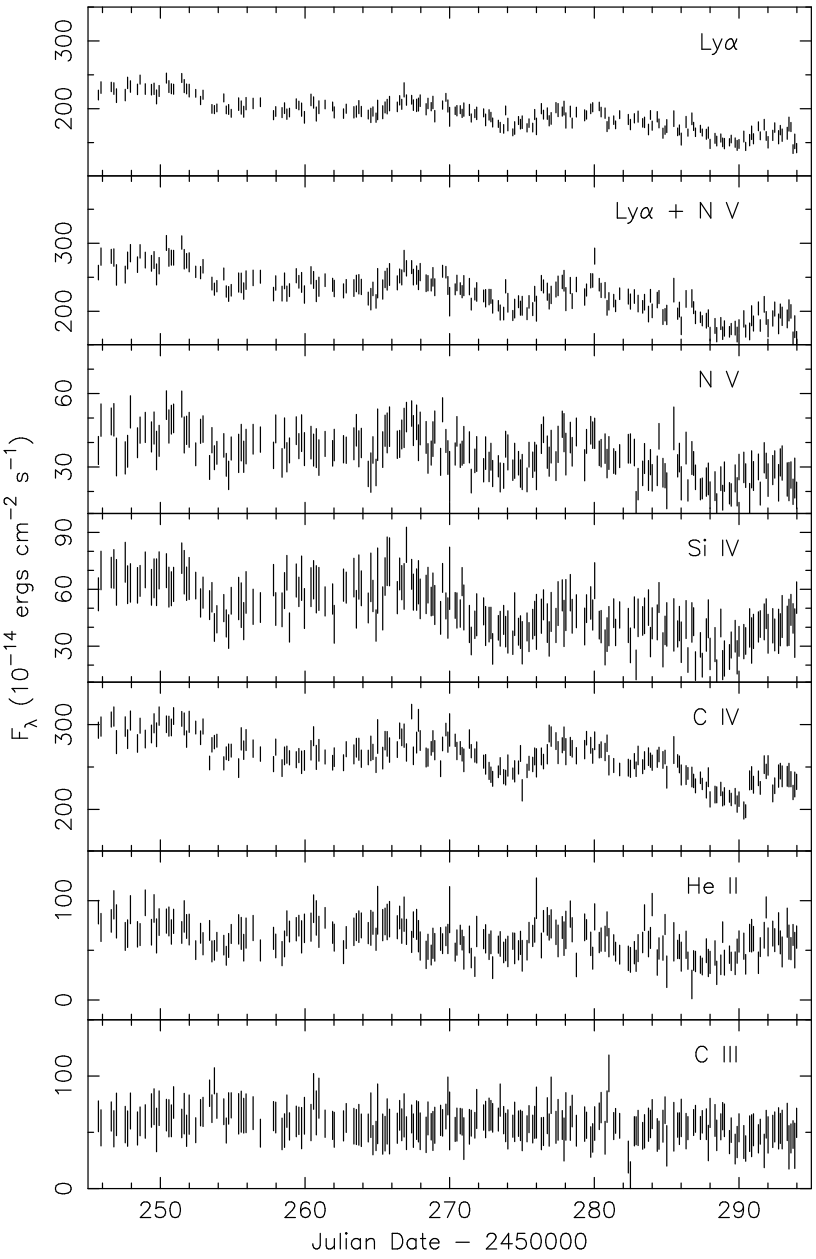


FIG. 4*b*

emission lines is not perfect. The nonvariable C III] line shows a nearly flat CCF with no significant peak. The other emission lines all show a maximum correlation coefficient of about 0.7. The centroid of the Lyα CCF has a lag of about $2^d.3$–$3^d.1$ (NEWSIPS–TOMSIPS, respectively). At least two features can be easily identified by inspection of the light curves (the maximum in the continuum flux at JD ≈ 264 and the minimum at JD ≈ 288) where the Lyα line indeed seems to respond with a delay of about $2^d.5$. Similarly, the lag for C IV is $\sim 2^d.7$, for Si IV the lag is $\sim 1^d.7$–$1^d.8$, and the He II lag is $\sim 0^d.7$–$1^d.0$. The N V lag is $1^d.9$–$2^d.4$, but this result may be significantly contaminated by the underlying red wing of the Lyα line, for which no attempt at correction has been made.

The uncertainties in the lag determinations for the emission lines are larger than for the continuum, up to $\sim 0^d.8$ for Lyα, based on the difference between the lags measured from the TOMSIPS- and NEWSIPS-derived spectra.

## 4. DISCUSSION

The existence of time delays between the different continuum bands is a potentially important result. For example, models for continuum reprocessing regions, where the lower energy photons are reprocessed higher energy photons originating closer to the source, predict wavelength-dependent time delays. However, a contaminant broad emission feature, such as the "small blue bump" that is attributable to a blend of Balmer continuum emission and a large number of Fe II lines, with a delayed response to the continuum variations, may also result in wavelength-dependent time delays if the relative strength of such an emission feature with respect to the continuum is a function of wavelength. In the case of NGC 5548, it has been shown that the small blue bump varies in response to continuum variations with a response time similar to that of Lyα and C IV (Maoz et al. 1993); if the same situation holds

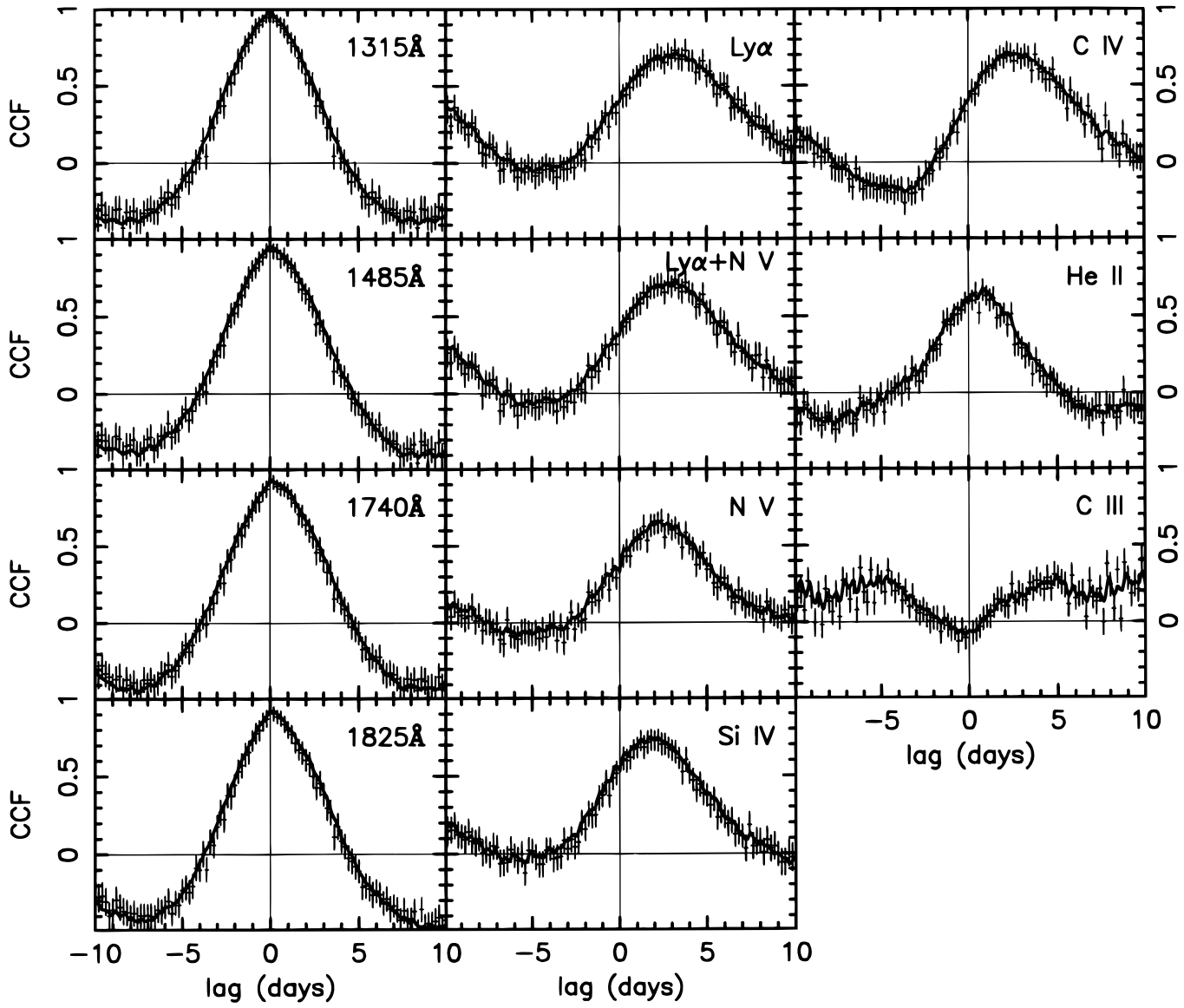


FIG. 5.—Continuum and emission-line CCFs of the TOMSIPS-reduced NGC 7469 data. Each light curve is correlated with the continuum light curve at 1315 Å. The ICCF is shown as a solid line and the DCF is shown as error bars.

TABLE 5

CROSS-CORRELATION RESULTS

| | NEWSIPS | | | | TOMSIPS | | | |
|---|---|---|---|---|---|---|---|---|
| FEATURE (1) | $r_{max}$ (2) | FWHM (days) (3) | $\tau_{peak}$ (days) (4) | $\tau_{cent}$ (days) (5) | $r_{max}$ (6) | FWHM (days) (7) | $\tau_{peak}$ (days) (8) | $\tau_{cent}$ (days) (9) |
| $F_\lambda$(1315 Å) (ACF)..... | 1.00 | 5.10 | 0.00 | 0.00 | 1.00 | 4.94 | 0.00 | 0.00 |
| $F_\lambda$(1485 Å)..... | 0.92 | 5.37 | 0.22 | 0.22 | 0.95 | 5.16 | 0.06 | 0.19 |
| $F_\lambda$(1740 Å)..... | 0.91 | 5.21 | 0.08 | 0.38 | 0.93 | 5.10 | 0.08 | 0.32 |
| $F_\lambda$(1825 Å)..... | 0.91 | 5.18 | 0.22 | 0.35 | 0.92 | 4.91 | 0.08 | 0.22 |
| Lyα..... | 0.71 | 7.33 | 2.10 | 2.32 | 0.71 | 6.91 | 3.26 | 3.10 |
| Lyα + N v ..... | 0.73 | 7.00 | 2.10 | 2.27 | 0.72 | 6.79 | 3.20 | 2.93 |
| N v..... | 0.68 | 6.09 | 2.10 | 1.90 | 0.66 | 5.34 | 2.20 | 2.39 |
| Si IV..... | 0.76 | 6.52 | 1.66 | 1.74 | 0.75 | 6.41 | 1.70 | 1.83 |
| C IV ..... | 0.69 | 7.14 | 2.20 | 2.72 | 0.71 | 5.70 | 2.20 | 2.70 |
| He II ..... | 0.53 | 4.83 | 0.92 | 0.99 | 0.67 | 4.64 | 0.80 | 0.70 |
| C III] ..... | 0.25 | ... | ... | ... | 0.32 | ... | ... | ... |

in NGC 7469, the continuum delays might be plausibly attributed to contamination by the small blue bump, which would be expected to follow the driving continuum with a short ($\sim$2–3 days) time delay.

In order to test how contamination by a time-delayed component might affect the lags measured in this experiment, we performed Monte Carlo simulations with the 1315 Å light curve as the driving light curve. The responding light curve was built from two components: an undelayed copy of the driving light curve and a delayed copy of the driving light curve. The delay was varied in steps of $0^d.1$, and the strength of the delayed copy (the contaminant) was varied from 2% to 10% with respect to the undelayed copy. The fluxes of both the driving and responding light curve were randomly reshuffled using Gaussian deviates determined from the error estimates for each datum, and the experiment was performed 20 times for each set of parameters. We find that the contaminant must be at least 10% as strong as the nondelayed responding light curve in order to have a significant effect on the lag determinations; even in this case, if the contaminant has a time delay as large as 2 days, the measured lag of the contaminated light curve will be only $0^d.19$, slightly smaller than the wavelength-dependent continuum lags we have found for NGC 7469. The measured lag will not increase any further when the lag of the contaminant is increased, owing to the way we calculate the position of the centroid of the CCF, which is defined at 0.8 times the peak value of the CCF; at larger lags, a secondary peak of the CCF, the signature of the contaminant, appears and is resolved. For larger lags, the contaminant is therefore directly identifiable in the CCF.

These contamination tests were done using a displaced version of the driving light curve as a contaminant. In other words, the transfer function of the contaminant was a delta function. We also performed simulations with a transfer function of the contaminant that was flat and extended over time delays 0–2$\tau$ (i.e., the transfer function for an isotropically emitting thin spherical shell of radius $c\tau$). In this model, the lag measurements are significantly smaller than those with a delta-function transfer function, and a contaminant with a time delay of 2 days and a strength of 10% of the uncontaminated light curve produces observed lags of only $0^d.15$.

Narrow spectral features that contaminate the continuum flux bins with a strength of 10% of the continuum variations can be ruled out from their nondetection in the rms spectrum (Fig. 1). However, we cannot eliminate contaminants that are broadly distributed over much of the width of the whole spectrum and therefore are indistinguishable from the actual continuum, e.g., strong Fe II emission that is clearly seen in the simultaneous *HST* spectrum (Kriss et al. 1997). A key test for the latter is that it implies that there should be no significant time delay between the UV at 1315 Å and the optical continuum at around 5100 Å. This prediction will be tested in a follow-up paper presenting the simultaneous optical monitoring campaign (Collier et al. 1997).

To provide a broader visual impression of the delays present in the spectra as a function of wavelength, we have rebinned all NEWSIPS and TOMSIPS spectra in bins of 20 Å per pixel and have cross-correlated each wavelength-bin light curve with the continuum light curve at 1315 Å. Figure 6 presents the maximum correlation coefficient and the centroid of the ICCF as a function of wavelength for both the NEWSIPS (*thin line*) and TOMSIPS (*thick line*) data.

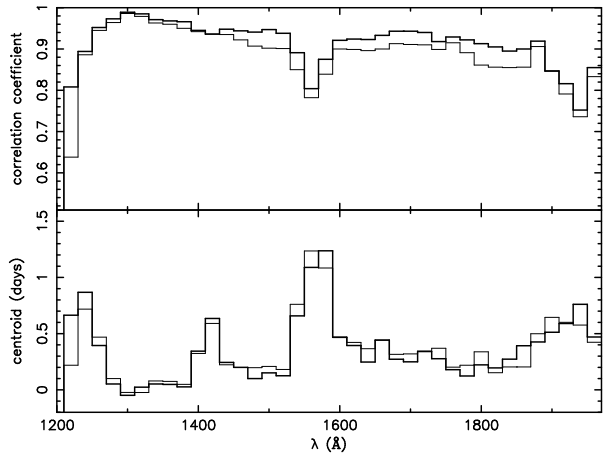


FIG. 6.—Maximum correlation coefficient and the centroid of the ICCF as a function of wavelength for the 1996 monitoring campaign on NGC 7469. Each light curve is defined by a 20 Å wide wavelength bin and is correlated with the continuum at 1315 Å. The thick line shows the TOMSIPS results, the thin line the NEWSIPS results.

The maximum correlation coefficients are smaller for the NEWSIPS data set than for the TOMSIPS data set. The TOMSIPS extraction procedure (Ayres 1993) does a superior job of removing fixed pattern noise, yielding smoother and less noisy light curves than those we obtain from the NEWSIPS spectra. We therefore place more confidence in the TOMSIPS results than in the NEWSIPS results.

The maximum correlation coefficient decreases at the position of the emission lines in the spectrum. This is because the lines respond with a longer lag to the driving light curve than the underlying continuum does. The two variable parts interfere with each other, which results in a decrease of the correlation coefficient.

Both NEWSIPS and TOMSIPS centroid determinations are strongly suggestive of a change in CCF centroid as a function of wavelength *outside* the emission-line wave bands. The wavelength regions of the spectrum where the continuum variations totally dominate the emission-line variations (see the rms spectrum in Fig. 1) are 1300–1380 Å, 1460–1540 Å, and longward of about 1720 Å. Even though the C III] emission line contaminates the continuum spectrum longward of 1900 Å, this line is known to be nonvariable on the timescales investigated here. The CCF is insensitive to additive constant components, and the lag determinations in this part of the spectrum may thus be attributed to the continuum or to other broadly distributed emission components.

From Figure 6, we can again estimate the uncertainty in the continuum lag determinations, as well as obtain an estimate of the significance of the result that the continuum lag is wavelength dependent. We can assume that the lag determinations between wavelength bins are independent. Thus we can estimate the error *per bin* to be the root mean square around the mean lag over $N$ wavelength bins. We can identify three continuum wavelength regions in Figure 6: 1300–1380 Å, 1480–1520 Å, and 1680–1940 Å (regions 1, 2, and 3, respectively). Table 6 shows the results of the average lag and estimated error per bin for the three continuum regions. Column (1) shows the continuum region; column (2), the

TABLE 6

CCF LAG ERROR ESTIMATES

| Region (1) | Number of Bins (2) | $\lambda_{center}$ (Å) (3) | ⟨lag⟩ (days) (4) | $\sigma$ (days) (5) |
|---|---|---|---|---|
| 1 ..... | 5 | 1340 | $0.02 \pm 0.02$ | 0.04 |
| 2 ..... | 3 | 1500 | $0.13 \pm 0.02$ | 0.03 |
| 3a ..... | 5 | 1740 | $0.23 \pm 0.04$ | 0.08 |
| 3b ..... | 5 | 1820 | $0.24 \pm 0.04$ | 0.10 |
| 3a+b ..... | 14 | 1810 | $0.34 \pm 0.05$ | 0.18 |

number of 20 Å wide bins; column (3), the wavelength at which the bins are centered; column (4), the average lag over the bins; and column (5), the root mean square $\sigma$ around the average lag, i.e., the error estimate of the lag determination per bin. The error estimates are rather upper limits than true estimates because we assume the lag is constant within each wavelength region. We find that the weighted average of the error estimates of the four non-overlapping wavelength regions (1, 2, 3a and 3b; see Fig. 6) is consistent ($0^d.08$) with the Monte Carlo derived estimate of the uncertainty in the continuum lag determination ($0^d.07$).

Besides estimating the errors in the determination of the CCF lag within an individual 20 Å wavelength bin, we can also test for the significance of the result that the CCF lags are wavelength dependent. Our null hypothesis is that the continuum lag is constant over the whole spectrum. The constant can be obtained from the data by least-squares fitting to the three previously defined continuum wave bands of Figure 6. We assign a 1 $\sigma$ error bar of $0^d.07$ to the lag $\tau$.

The number of degrees of freedom, $\nu$, of the fit is the number of wavelength bins minus the number of fitted parameters, i.e., $\nu = 22 - 1 = 21$. It equals the expectation value of the $\chi^2$ statistic if the model that is being fitted is good. The $\chi^2$ statistic is our measure of goodness of fit and is found to be 133 for the null hypothesis. The incomplete gamma function $Q \equiv Q(\nu/2, \chi^2/2)$ measures the probability $Q$ that the $\chi^2$ is larger than its value by chance. [For a discussion of $Q(\nu/2, \chi^2/2)$, see Press et al. 1992.] A small value of $Q$ ($\lesssim 10^{-8}$) thus signifies a very poor fit, whereas a large value of $Q$ ($\gtrsim 10^{-3}$) signifies a reasonable to good fit. For $\chi^2 = 133$ and $\nu = 21$, $Q \ll 10^{-8}$ and the null hypothesis can be ruled out as a good representation of the data with great confidence.

## 5. SUMMARY

A 7 week continuous monitoring campaign on the Seyfert 1 nucleus NGC 7469 was conducted with the *IUE* satellite during 1996 June–July. Significant continuum variability was detected, and the emission lines also varied but with much smaller amplitude. The results can be summarized as follows.

1. The continuum light curves exhibit a wavelength-dependent lag relative to the continuum variations at 1315 Å: $\tau \approx 0^d.19$ at 1485 Å, $0^d.32$ at 1740 Å, and $0^d.22$ at 1825 Å for the TOMSIPS-reduced data, and $0^d.22$, $0^d.38$, and $0^d.35$, respectively, for the NEWSIPS-reduced data. The average lags are $0^d.21$, $0^d.35$, and $0^d.28$, respectively. The presence of wavelength-dependent continuum lags is further demonstrated by a more detailed analysis over all wavelengths in the spectra (Fig. 6). We estimate through Monte Carlo simulations that the uncertainty in these determinations is about $0^d.07$, although we emphasize that there is no general agreement about how such uncertainties should be determined. Furthermore, on the basis of the UV data alone, we are unable to determine definitively whether the lags are due (1) to actual wavelength dependence of the continuum variations, as might be expected if the UV continuum at longer wavelengths is reprocessed emission from shorter wavelength photons, or (2) to contamination of the measured continuum by a very broad, delayed emission feature, such as the "small blue bump," which becomes progressively stronger toward the red part of the spectrum. Concurrent optical observations (Collier et al. 1997), combined with these data, will provide a more definitive test of the reality of this phenomenon, and if it is indeed real, much stronger constraints on its possible origin.

2. The amplitude of the continuum variations at the longer wavelengths is smaller than at the shorter wavelengths, which thus confirms the results of previous studies.

3. The Ly$\alpha$, Si IV, and C IV emission lines lag behind the continuum variations by about $2^d.3$–$3^d.1$, whereas the He II line has a lag of about $0^d.7$–$1^d.0$, and the C III] line does not respond to the rapid continuum variations at all. The variable part of the broad lines arises in gas at a typical distance of about 3 lt-days from the continuum source.

4. All emission lines show a decreasing trend in their total flux from the beginning to the end of the monitoring campaign. This trend is also seen in the continuum fluxes and may be attributed to much longer continuum-variability timescales.

We gratefully acknowledge support for this work by NASA through grants NAG 5-2477 and NAG 5-3497.

## REFERENCES

Alloin, D., Clavel, J., Peterson, B. M., Reichert, G. A., & Stirpe, G. M. 1994, in Frontiers of Space and Ground-Based Astronomy, ed. W. Wamsteker, M. S. Longair, & Y. Kondo (Dordrecht: Kluwer), 325
Ayres, T. R. 1993, PASP, 105, 538
Blandford, R. D., & McKee, C. F. 1982, ApJ, 255, 419
Clavel, J., et al. 1991, ApJ, 366, 64
Collier, S., et al. 1997, in preparation
Collin-Souffrin S. 1991, A&A, 249, 344
Courvoisier, T. J.-L., & Clavel, J. 1991, A&A, 248, 389
Crenshaw, D. M., et al. 1996, ApJ, 470, 322
Dietrich, M., et al. 1993, ApJ, 408, 416
Edelson, R. A., et al. 1996, ApJ, 470, 364
Edelson, R. A., & Krolik, J. H. 1988, ApJ, 333, 646
Edelson, R. A., Krolik, J. H., & Pike, J. F. 1990, ApJ, 359, 86
Gaskell, C. M., & Peterson, B. M. 1987, ApJS, 65, 1
Gaskell, C. M., & Sparke, L. S. 1986, ApJ, 305, 175
Harris, A. W., & Sonneborn, G. 1987, in Exploring the Universe with the *IUE* Satellite, ed. Y. Kondo (Dordrecht: Kluwer), 729
Horne, K., Welsh, W. F., & Peterson, B. M. 1991, ApJ, 367, L5
Kassebaum, T. M., Peterson, B. M., Wanders, I., Pogge, R. W., Bertram, R., & Wagner, R. M. 1997, ApJ, 475, 106
Kaspi, S., et al. 1996, ApJ, 470, 336
Koratkar, A. P., & Gaskell, C. M. 1991, ApJS, 75, 719
Korista, K. T., et al. 1995, ApJS, 97, 285
Kriss, G. A., et al. 1997, in preparation
Krolik, J. H., & Done, C. 1995, ApJ, 440, 166
Krolik, J. H., Horne, K., Kallman, T. R., Malkan, M. A., Edelson, R. A., & Kriss, G. A. 1991, ApJ, 371, 541
Maoz, D., et al. 1993, ApJ, 404, 576
Nandra, K., et al. 1997, in preparation

Nichols, J. S., Garhart, M. P., de la Peña, M. D., & Levay, K.L. 1993, NEWSIPS Information Manual: Low-Dispersion Data v1.0, CSC/SD-93/6062
Peterson, B. M. 1993, PASP, 105, 247
Peterson, B. M., et al. 1991, ApJ, 368, 119
Press, W. H., Teukolsky, S. A., Vetterling, W. T., & Flannery, B. P. 1992, Numerical Recipes (2d ed.; Cambridge: Cambridge Univ. Press)
Reichert, G. A., et al. 1994, ApJ, 425, 582
Rodríguez-Pascual, P. M., et al. 1997, ApJS, 110, 9
Romanishin, W., et al. 1995, ApJ, 455, 516
Salamanca, I., Alloin, D., & Pelat, D. 1995, A&AS, 111, 283
Santos-Lleó, M., et al. 1997, ApJS, in press
Stirpe, G. M., et al. 1994, ApJ, 425, 609
Wanders, I., et al. 1995, ApJ, 453, L87
Warwick, R. S., et al. 1996, ApJ, 470, 349
Welsh, W. F., et al. 1997, in preparation
White, R. J., & Peterson, B. M. 1994, PASP, 106, 879